NASA Technical Memorandum 4330

Aerothermal Test Results From the First Flight of the Pegasus Air-Launched Space Booster

Gregory K. Notiz, Robert E. Curry,
Edward A. Haering, Jr., and Paul Kolodziej

OCTOBER 1991

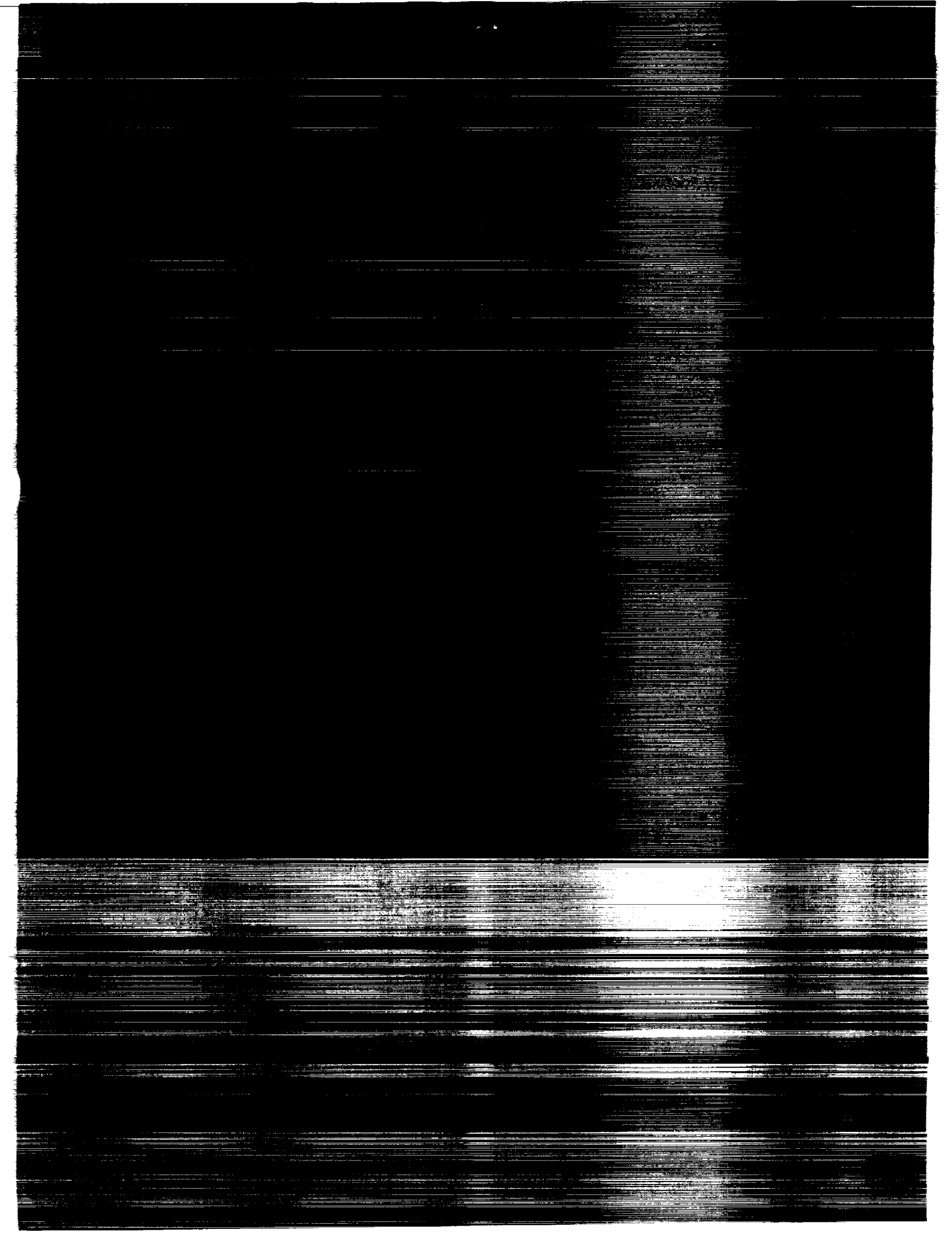

NASA Technical Memorandum 4330

Aerothermal Test Results From the First Flight of the Pegasus Air-Launched Space Booster

Gregory K. Noffz, Robert E. Curry,
and Edward A. Haering, Jr.
Dryden Flight Research Facility
Edwards, California

Paul Kolodziej
Ames Research Center
Moffett Field, California

National Aeronautics and
Space Administration

Office of Management

Scientific and Technical
Information Program

1991

Use of trade names or names of manufacturers in this report does not constitute an official endorsement of such products or manufacturers, either expressed or implied, by the National Aeronautics and Space Administration.

CONTENTS

ABSTRACT

A survey of temperature measurements was obtained at speeds through Mach 8.0 on the first flight of the Pegasus® air-launched booster system. In addition, heating rates were derived from the temperature data obtained on the fuselage in the vicinity of the wing shock interaction. Sensors were distributed on the wing surfaces, leading edge, and on the wing-body fairing or fillet. The majority of sensors were thin foil temperature gages installed near the surface within the vehicle's thermal protection system. In regions below the thermal protection system, standard bulb thermocouples were employed. In addition to these gages, thermocouples were installed on the surface of non-ablating plugs. These sensors were more responsive to changes in flight conditions than the foil gages and allowed a derivation of convective heat flux. Side-by-side evaluations were obtained for a variety of sensor installations. Details of the trajectory reconstruction through first-stage separation are provided. This paper provides indepth descriptions of the sensor installations, temperature measurements, and derived heating rates along with interpretations of the results.

INTRODUCTION

The first orbital insertion mission of the Pegasus® air-launched booster system was conducted successfully on April 5, 1990. The Pegasus vehicle was developed as a private joint venture by Orbital Sciences Corp. and Hercules Aerospace Corp., Magna, Utah. The vehicle uses aerodynamic forces for lift and control at speeds through Mach 8.0. During the development phase, the Pegasus configuration was never tested in a wind tunnel, resulting in substantial time and cost savings (ref. 1).

Such an approach, however, required heavy reliance upon analytic tools used in the aerodynamic and thermal protection design process. The research objective of instrumenting flights no. 1 and no. 2 is to evaluate the overall effectiveness of the aerothermal design tools, develop flight test techniques on an ablating vehicle, and provide empirical information related to specific hypersonic flow features of the configuration. Specific conclusions about the analytic predictions are pending until the predictions are adjusted for the actual flight no. 1 trajectory.

The purpose of this paper is to present the results of the flight no. 1 instrumentation effort, including details on the unique sensor installation process. This presentation will be part of the information required to meet the overall objectives of the flight test program.

A research instrumentation system, developed by the National Aeronautics and Space Administration (NASA), was installed in the first stage of the vehicle. This system was carried along as an "add-on" experiment and was constrained to have minimal impact on either the primary payload mission or the flight operation. Data obtained from the research system were correlated with flight conditions, determined through an extensive postflight trajectory analysis conducted using radar, balloon, and inertial data.

The research system included temperature sensors distributed on the wing surfaces, leading edge, and the wing-body fairing (or fillet). The majority of sensors were embedded in the ablating thermal protection system (TPS) causing minimal perturbation of the local structure and thermal boundary layers. These sensors can provide direct measurements for comparison with analytic predictions.

In addition, some thermocouples were mounted on plugs fabricated from highly insulative, nonablating material. The plug surface temperatures were expected to respond rapidly to local aerothermal conditions and were used to derive estimates of convective heat flux. The plugs were fabricated from well-characterized materials that could be modeled analytically. Potential advantages of the plug concept for future applications include fabrication to conform to complex surface shapes and the support of a variety of surface sensors.

® Pegasus is a registered trademark of Orbital Sciences Corp., Fairfax, Virginia.

The distribution of the plug-mounted sensors was selected to identify the effects of the shock wave and compression field generated by the wing at the sidewall of the fuselage-wing fairing. Because of the variation of Mach number and angle of attack during the flight, a wide range of wing-body flow conditions were present.

This paper provides a detailed description of the design and installation of the flight instrumentation and analysis of the test results obtained from the first Pegasus mission. A similar experiment (which will also include surface pressure measurements) is planned for the second flight.

The authors would like to acknowledge the monetary support of the Defense Advanced Research Project Agency (DARPA).

NOMENCLATURE

b	wing span, in.
C_p	specific heat, Btu lb_m^{-1} °F^{-1}
c	local wing chord, in.
EMF	electromotive force
FS	fuselage station, in.
g	acceleration due to gravity at sea level, 32.1740 ft sec^{-2}
HRSI	high-temperature reusable surface insulation
$Heat_{abl}$	heat of ablation, Btu lb_m^{-1}
H_z	Hertz, c sec^{-1}
INS	inertial navigation system
k	thermal conductivity, Btu in^{-1} sec^{-1} °F^{-1}
LTA	Lockheed Thermal Analyzer
M	Mach number
MUX	multiplex device
NWS	National Weather Service
P_S	static pressure, lb in^{-2}
q	heat flux, Btu ft^{-2} sec^{-1}
$\bar{q}$	dynamic pressure, lb ft^{-2}
q_{cond}	conductive heat flux into wall from surface, Btu ft^{-2} sec^{-1}
q_{conv}	convective heat flux to the surface, Btu ft^{-2} sec^{-1}
q_{rad}	radiative heat flux, Btu ft^{-2} sec^{-1}
q_{ref}	reference surface convective heat flux, Btu ft^{-2} sec^{-1}
R	ideal gas constant, 53.35 $\frac{\text{ft lb}}{\text{°R lb}_m}$
T_{abl}	ablation temperature, °F
T_{act}	activation temperature, °F
T_s	surface temperature, °R
T_∞	ambient temperature, °R
T	temperature, °F

TC	thermocouple
TPS	thermal protection system
t	time from launch, sec
t_{skew}	time lag, sec
u	axial airspeed component (positive forward), ft/sec
V	velocity, ft/sec
v	lateral airspeed component (positive right), ft/sec
W	wind velocity, ft/sec
w	vertical airspeed component (positive down), ft/sec
x	local longitudinal coordinate, measured aft from leading edge, in.
y	lateral coordinate, measured to the right from vehicle centerline, in.
Z	geometric altitude, ft
z	vertical coordinate, measured up from vehicle thrust line, in.

Subscripts

abl	ablation
act	activation
D	down
E	east
N	north
∞	free stream

Greek symbols

α	angle of attack, deg
β	angle of sideslip, deg
Γ	Euler rotation transformation matrix
γ	ratio of specific heats for air, 1.4
Δ_q	incremental difference in convective heat flux, Btu ft^{-2} sec^{-1}
ε	emissivity
ζ	damping ratio
θ	pitch angle, deg
ρ	density, lb_m ft^{-3}
σ	Stefan-Boltzmann constant, 3.3063×10^{-15} Btu in^{-2} sec^{-1} $°R^{-4}$
ϕ	roll angle, deg
Ψ	yaw angle, deg
ω	cut-off frequency of filter

VEHICLE DESCRIPTION

The Pegasus vehicle is an air-launched, winged, three-stage expendable solid rocket booster system intended to deliver payloads of up to 900 lb into low Earth orbit. The launch configuration is shown in figure 1, along with a photograph of the booster mated to the B-52 carrier aircraft. The wing, tail surfaces, and wing-body fillet are all included on the first stage. Research instrumentation components described in this report were installed on the first stage of the flight no. 1 vehicle. Total weight at launch for the flight no. 1 vehicle was 41,765 lb.

The flight no. 1 mission began with the take-off of the B-52–Pegasus from Edwards Air Force Base, California. The Pegasus air-launched space booster was released from the B-52 aircraft off the coast of Monterey, California at an altitude of approximately 42,000 ft and a speed of Mach 0.8. After ignition, the Pegasus vehicle continued on a southerly heading to an altitude of approximately 220,000 ft and a speed of approximately Mach 8.2. At this point, the first stage separated from the rest of the vehicle. The Pegasus vehicle went on to deliver its payload to a polar low Earth orbit.

The Pegasus wing is nearly triangular in planform with zero dihedral and a 45° leading-edge sweep. The airfoil sections at lateral coordinate (y) = 65 in. and y = 32 in. are shown in figures 2(a) and (b), respectively. The airfoil is a truncated diamond type with a nominal 1-in.-radius leading edge. The wing skin is a sandwich constructed of foam surrounded by two layers of graphite-epoxy. The wing leading edge is constructed only of graphite-epoxy and has a nominal thickness of 0.125 in.

The wing-body fillet provides an aerodynamic fairing between the wing and the cylindrical rocket motor casing. The fillet construction is similar to that of the wing skin.

The Pegasus thermal protection system (TPS) consists of insulative and ablative materials in various combinations applied to the external surface of the graphite-epoxy substructure. Four materials were used: Firex RX-2376A (Pfizer Minerals, Pigments and Metals Division, New York, New York), Thermolag T-230 (Thermal Science, Inc., St. Louis, Missouri), cork phenolic, and an Acurex-developed spray-on insulator (Acurex Corp., Huntsville, Alabama). Thermal properties of these materials are given table 1. Firex is a polymer ablative material that begins to melt and flow at approximately 250 °F. Thermolag is an ablative material that sublimes at a temperature of approximately 230 °F. Both ablative materials were sprayed on. Cork was obtained in 0.04-in.-thick pressed sheets and glued in place. The Acurex insulator consisted of glass microballoons suspended in an epoxy resin. Once sprayed, the insulator begins to set, and eventually hardens to a brittle foam. Specific details of the TPS as applied at the various sensor installations will be described in the next section.

INSTRUMENTATION

The research instrumentation system consisted of 86 chromel-alumel (type K) thermocouples (TCs) and related signal conditioning hardware. A summary of sensor distribution is given in table 2.

Wing Upper and Lower Surface Foil Installations

A total of 28 thin "foil" TCs were installed in the wing surface TPS. These sensors were approximately 0.006 in. thick and encased in a polyimide laminate, see figure 3. The geometry of these TCs allowed temperature measurements within the thin layers of the TPS.

The original TPS design for the wing surfaces consisted of a 0.040-in. layer of Acurex insulator and an external layer of 0.015-in. Firex ablative material. A single foil TC was built into the interface between the Firex and the insulator at the majority of sensor locations. At some locations, however, TCs were also installed between the graphite-epoxy and insulator. See figure 4 for wing sensor locations and local TPS configurations.

The objective of the foil installations was to provide measurements directly comparable to preflight predictions. Consequently, the installation of the sensors could not greatly perturb the local structure, TPS configuration, or local thermal boundary layer. The foil installation process required only a 0.125-in.-diameter hole in the graphite-epoxy structure at the desired locations. The foil TCs were then bonded to each successive layer with the leads routed down through the hole. The TC junction was located approximately 0.75 in. away from the hole and any effect of the hole on the heat path through the structure is assumed negligible.

After the foil gages were installed, the wing surface TPS design was modified. Square patches of the original thermal protection surrounding the gages, approximately 2 in. on each side, were left intact while the remaining wing TPS was removed. This material was replaced with a 0.04-in.-thick layer of cork and a 0.015-in.-thick layer of Firex. The transition between the new TPS surface with the old TPS patches (which included the foil gages) was sanded smooth.

Wing Leading-Edge Foil Installations

As shown in figure 4, the thermal protection on the wing leading edge consists of one layer of Firex approximately 0.060 in. thick. Leading-edge sensor locations also can be found in figure 4. Most leading-edge installations consisted of a single TC, but at three locations a second TC was bonded on the structure prior to any Firex application. The installation procedure was similiar to the other wing installations.

Fillet Foil Installations

All fillet instrumentation locations are diagramed in figure 5. On the fillet, the TPS consisted of 0.015-in.-thick Thermolag ablator on a 0.04-in. layer of cork insulator. The installation procedure for foil TCs was similar to the procedure used on the wing.

Bulb Thermocouple Installations

These TCs were fabricated from standard 30 gage type K TC wire. The thickness of these TCs precluded their use in the TPS, but they were suitable for installation on the graphite-epoxy backwall. Bulb TCs were also installed on the signal conditioning equipment.

To install a bulb TC just inside the exterior layer of the carbon-graphite, a 0.125-in. hole was drilled through the interior layer of carbon-graphite and the sandwiched foam, but not the exterior layer. A bulb TC was inserted, pressed against the inside of the exterior surface and backfilled with epoxy and microballoons. Because of space limitations the TC leads could not be laid in contact with the graphite-epoxy surface. This is an important distinction from the previous foil installations where the TC leads were perpendicular to the direction of heat flow. Whenever TCs are installed so their leads are parallel to the direction of heat flow, a certain amount of heat undoubtedly will be conducted down the leads themselves, resulting in a lower temperature at the TC junction. This issue and its relevance to the bulb installations will be addressed in the Discussion of Results section.

High-Temperature Reusable Surface Insulation Plugs

Ten TCs were fabricated from small-diameter (0.005 in.) wires, which were mounted on the surface of 1-in.-diameter, 0.4-in.-thick plugs (see fig. 6(a)). The plugs were solid pieces of shuttle tile material, LI2200. Details of the material properties are given in table 3. A high-temperature, high-emissivity coating was applied over the TCs. After measurement with a spectrophotometer the emissivity of the coating was determined to be 0.85. Samples of the coating were heated in ground facilities to temperatures of 600 °F and no degradation in emissivity was observed.

The installed configuration of the plugs is shown in figure 6(b). Indentations were provided in the structure itself at locations where plugs were to be installed. The structure and thermal boundary layer were perturbed far more than in the case of the foil gages, but a more reliable heat flux measurement resulted at the surface.

Signal Conditioning

The signal from each TC was input to a 32 °F reference junction and a 10-Hz low-pass filter. The filtered analog signals were then input to a multiplex (MUX) unit. The MUX output was merged with the Pegasus data stream and telemetered to a ground station.

There were two MUX units dedicated to the research instrumentation, one for the wing sensors, and one for the fillet sensors. These were identical to others used in the Pegasus vehicle and allowed easy integration of the research data into the basic Pegasus telemetry data stream. Research measurements were limited, however, because of the resolution and sampling capabilities of the MUX units, as well as the total available bandwidth. The MUX units digitized the data into 8-bit words at a rate of 5 samples/sec. All foil and bulb TCs were ranged from −115 to 320 °F. The HRSI plug TCs were ranged from −115 to 2300 °F.

All signal conditioning hardware was located in the enclosed fillet volume. Five TCs were mounted in and around the signal conditioning components to monitor their temperature. These TCs verified that the hardware remained at essentially constant temperatures ($35 < T < 48$ °F) throughout the flight.

TRAJECTORY

Figures 7(a) through (e) show pressure altitude, free-stream Mach number, free-stream dynamic pressure, angle of attack, and angle of sideslip, respectively. Details of the postflight trajectory derivation are given in the appendix.

HEAT FLUX DERIVATION FROM HIGH-TEMPERATURE REUSABLE SURFACE INSULATION PLUGS

The HRSI plugs were analytically modeled using the Lockheed Thermal Analyzer (LTA) program (Lockheed Report 18902, *Thermal Analyzer Computer Program for the Solution of General Heat Transfer Problems*). The LTA program was used to determine the conduction and radiation components from the temperature time histories measured at the plug surfaces. This finite element code solves transient thermal problems in up to three dimensions. Shown in figure 8 is the LTA model of the shuttle tile plugs used in this analysis. Because of the plugs' large width, heat conduction in the lateral direction was assumed negligible and a one-dimensional model sufficed. Computed temperature profiles indicated that because of the plugs' depth, it was not necessary to model a heat path on the backside of the plugs. Thinner elements were used near the surface that experienced higher temperature gradients. The HRSI thermal conductivity was input as a function of temperature and static pressure (table 3). Specific heat of HRSI varied with temperature alone.

The nonablating HRSI surface has only three heat transfer modes at the surface: convection, conduction, and radiation. No energy leaves the surface in the form of ablation products. Given the surface temperature and assuming a view factor of 1.0 and a 0.0 °R reservoir, radiation heat transfer was determined from the Stefan-Boltzmann equation:

$$q_{rad} = \varepsilon \sigma T_s^4$$

Using the surface temperature time history, the heat conduction into the wall can be determined from a finite element model such as the one used in the LTA program, and is based on

$$q_{cond} = -k\left(\frac{dT}{dx}\right)_{x=0}$$

The convective heat flux at the surface is then the sum of the radiative and conductive heat fluxes,

$$q_{conv} = q_{cond} + q_{rad}$$

provided the conduction component is defined as positive when heat is flowing into the material and the radiation component is defined as positive when energy is leaving the surface. A similiar procedure was used in the analysis of space shuttle thermal data (ref. 3). Other sources include references 5, 6, and 7.

The digitized temperature time histories from the plug surface were filtered prior to input into the LTA program. This filtering is performed postflight and is conducted in addition to the 10-Hz onboard filter discussed in the Signal Conditioning Section. A second-order Butterworth filter was used with a roll-off frequency appropriate for the level of noise on that channel (see table 4). Lags from the filtering process were compensated for by time skews using the formula

$$t_{skew} = 2 \times \frac{\zeta}{\omega}$$

where

$$\zeta = 0.707$$

Reference junction error (±1 percent), bit resolution (±0.4 percent), and TC electromotive force (EMF) error (±0.01 percent) combine for a root-sum-square error of ±1.07 percent in the temperature measurements alone. Uncertainty in the heat flux derivation stems primarily from uncertainties in the material properties of the shuttle tile material (conductivity, ±18 percent; specific heat, ±10 percent; density, ±9 percent). Emissivity error is assumed negligible. A root sum square of the errors of the terms in the energy balance equation gives an error of

$$q_{conv} = \pm 22.6 \text{ percent}$$

DISCUSSION OF RESULTS

Wing Thermal Protection System

Just prior to launch, all temperatures were at steady values between approximately −5 to −35 °F. All temperatures were indicating that the TPS and structure were cold-soaked to near atmospheric conditions and that there were no large instrumentation biases in the system. The lower surface wing temperature time histories measured at the Firex–insulator interface are shown in figures 9 and 10. For most channels, the noise is within one or two counts throughout the flight. Certain data channels, such as fuselage station (FS) = 245 in. on the outboard row (fig. 10(a)) experienced data dropouts at various times throughout the flight. In such instances, the temperature time history was linearly interpolated between the closest available points. Thirteen channels were affected to varying degrees and are identified on the figures.

In all cases, temperatures begin to rise approximately 10 sec after launch (figs. 9 and 10). The regions just aft of the leading edge on both inboard and outboard rows (figs. 9(a) and 10(a)) are at lower temperatures than regions farther aft (figs. 9(b) and 10(b)) on the windward panel. The six aft locations on the inboard row all leveled off at approximately 250 °F, the ablation temperature of Firex (Figs. 9(c) and 10(c)). On the inboard row, the second and third stations (FS = 283 in., FS = 273 in.) exceed the data range limit of 320 °F implying that the ablative material

was depleted in this area. This pattern is repeated on the outboard row with the second station (FS = 253 in.) not quite exceeding the range limit.

Figure 11 shows the comparison of the temperatures measured at various depths in the wing TPS at the same location. Note that prior to launch the graphite-epoxy inner wall is slightly warmer than the outer layers in most cases. As expected, the temperature rise of the lower sensors lags that of the sensor located nearest to the surface. The maximum temperature measured on the graphite-epoxy substructure never exceeded 230 °F.

The temperature difference between the inside and outside surfaces of the graphite-epoxy was much greater than anticipated. This result indicates that the inside bulb TC gages may not have had good contact with the surface or that the leads were conducting heat from the surface. Both of these effects would result in measuring cooler temperatures than were actually present in the surrounding material.

To better visualize the phenomena seen in figures 9 and 10, Firex–insulator interface temperatures are plotted as a function of chord for different times in figure 12. By 50 sec after launch, the majority of temperatures were approaching the ablation temperature of Firex (250 °F). Temperatures between chord location (x/c) = 0.10 and 0.30 continued to increase above 250 °F, indicating that the ablative layer was depleted in this region, as noted previously. At both chordwise locations, the sensor ahead of x/c = 0.10 indicated less severe heating.

Since data from the embedded TCs are expected to be sensitive to details of the sensor installation and TPS application processes, the consistency of the trends from the two chordwise distributions is considered good. The reason that higher temperatures were measured on the outboard row at x/c = 0.62 is not understood at this time, but it may be a result of the sensor installation. Preflight measurements of the surface smoothness at the various sensor locations did not indicate any anomalies at this particular installation.

Comparisons of the Firex–insulator interface temperatures on the upper and lower surface are presented in figure 13. As shown, initially the temperatures rose more sharply on the lower surface. The upper surface temperature-rise rate increased substantially at approximately t = 30 sec, at both span locations. This corresponds to the start of a pitch-down manuever from 7° to 0° angle of attack, see figure 7(d).

Time histories of the various leading-edge sensors are shown in figure 14. The temperatures measured here were generally lower than those measured along the chordwise rows because the TCs are situated deeper within the TPS. The initial temperatures were steady and similar to the chordwise sensor data. Note that certain channels experienced data dropouts and now contain regions of interpolation. Figure 15 shows the spanwise distribution of temperatures from TCs located at the midpoint of the ablative layer.

Fillet Thermal Protection System

The temperature time histories for the foil gages embedded in the fillet TPS are shown in figure 16. Initial temperatures for these sensors were similar to the wing sensors. Most of the sensors reached the ablation temperature of the Thermolag, (230 °F) which is slightly lower than the wing ablative material. Although some sensors exceeded the ablation temperature, all temperatures leveled out at no more than 270 °F. The temperature rise was generally more severe for sensors located closer to the lower surface of the wing. The temperature variations coincide roughly with pitch-down maneuvers in the trajectory data. The fillet sensor at FS = 253.1 in. and vertical coordinate (z) = 20.5 in. (fig. 16(e)) indicates large temperature variations during the flight. No explanation is available for the response of this particular sensor.

Fillet High-Temperature Reusable Surface Insulation Plugs

The measured surface temperature and derived convective heat flux for the various HRSI plugs are shown in figure 17. Initial temperatures were slightly higher than the TPS values and the plug data show more fluctuations

during the flight and higher maximum temperatures. Rapid surface response to external heating variations is expected since the HRSI plugs are not covered with ablative material and have highly insulative properties. Subtle variations in the temperature time histories, correspond to substantial heat flux variations. As seen with the foil TCs, the plugs begin to heat up at approximately 10 sec. Temperature steadily increases for all of the plugs until approximately 45 sec as shown in figure 17. A large heat flux pulse is shown by all the HRSI plug data at t = 76 sec, (fig. 17). The time and magnitude of this event is essentially the same for all plugs. This event coincides with the final seconds of first-stage motor operation.

The heat flux data must be interpreted with respect to the trajectory and sensor location. By using supersonic wedge tables (ref. 4) for several trajectory flight conditions, an estimate of the wing leading-edge shock-wave position, superimposed on the sidewall of the fillet, is shown in figure 18(a). This estimate does not account for offsets caused by the 1-in. wing leading-edge radius or fuselage bow shock effects. Based on this estimate, however, the three sensors at the forward corner of the fillet, farthest from the wing, are expected to be upstream of the wing shock at high Mach numbers. When compared, heat flux data for these sensors agree favorably throughout the flight profile, see figure 18(b). Therefore, data from these sensors will be referred to as the reference heating, q_{ref}, and used to normalize data from other fillet sensors.

Figure 19 shows the additional heating, which is defined as:

$$\Delta_q = q_{conv} - q_{ref}$$

for several fillet sensors. These sensors are located aft and close to the lower surface of the wing, and are therefore downstream of the estimated shock position at all flight conditions. Substantial additional heating is present for these sensors during the first half of the flight. The additional heating builds to a maximum at t = 45 sec, when the angle-of-attack pitch-down maneuver begins (see fig. 7). At t = 55 sec, this maneuver is complete, and angle of attack is approximately 0° for the remainder of the flight. Additional heating after t = 55 sec is also approximately zero.

Figure 20 shows the additional heating for the sensors located in the wing shock region. For most of these sensors, some additional heating is present during the portion of flight with angle of attack (t < 55 sec). After t = 55 sec, when angle of attack is 0°, these sensors indicate additional heating up to 0.47 Btu ft^{-2} sec^{-1}. It is hypothesized that this additional heating is caused by the proximity of the wing leading-edge shock. Other factors to be considered are the vehicle angle of sideslip (β) and Mach number. Angle of sideslip is approximately 0° during most of the high Mach number portion of the flight. During the period of peak additional heating caused by the shock, 60 < t < 65 sec, angle of sideslip approaches a value of $\beta \approx 1°$ (resulting in the right-hand side of the fillet being more windward).

Reference heating at t = 62 sec is approximately 0.50 Btu ft^{-2} sec^{-1}. The peak additional heating observed in this experiment of 0.47 Btu ft^{-2} sec^{-1} corresponds to a magnification factor of approximately 2 ($q_{conv}/q_{ref} \approx 2$). Perhaps follow-on Pegasus experiments will better define the significance of angle-of-sideslip effects, the local pressure field, and boundary-layer characteristics in this vicinity.

CONCLUDING REMARKS

Temperature measurements within the thermal protection system (TPS) of the first Pegasus® air-launched space booster have been presented. The TPS temperature measurements were obtained on the wing lower and upper surfaces, wing leading edge, and wing-body fillet. In addition, surface heat flux is calculated for the high-temperature reusable surface insulation (HRSI) plugs installed on the wing-body fillet. The data presented in this report, along with data to be obtained on flight no. 2, will be used to evaluate the effectiveness of the aerothermal design tools used in the development of the Pegasus vehicle and provide empirical information related to specific hypersonic flow features of the configuration.

® Pegasus is a registered trademark of Orbital Sciences Corp., Fairfax, Virginia.

Thin foil thermocouples (TCs) installed within the thermal protection system (TPS) have provided a way of obtaining temperature measurements within the thin layers of the Pegasus TPS. The HRSI plugs proved responsive to small variations in vehicle flight conditions and provided a heat flux measurement from a nonablating surface.

The thin foil TC data from the wing indicated consistent trends in the inboard and outboard rows. Most wing temperature time histories stabilized near the ablation temperatures, with the exception of sensors between 10 and 30 percent of the wing chord where the ablative material appears to have been depleted. The data from foil gages at lower depths in the TPS showed consistent lags because of the thermal capacitance of the TPS. A larger than expected lag was measured for the bulb gages at the inboard surface of the graphite-epoxy, which may be the result of an inadequate sensor installation procedure.

Temperatures measured within the fillet TPS were generally similar to the wing data, however, no sensors significantly exceeded the ablation temperature. Temperature-rise rates were slightly higher near the wing lower surface in the foil gage data and the HRSI plugs. This phenomenon probably resulted from increased compression in the wing flow field. As expected, the insulative properties of the plugs resulted in higher surface temperatures and more responsiveness to changes in flight conditions.

Derivations of convective heat flux from the HRSI plugs resulted in consistent trends for all sensors forward of the expected wing leading-edge shock position. Data obtained from sensors aft of the shock had additional heating characteristics that could be directly related to vehicle angle of attack and angle of sideslip. The maximum value of heating rate measured in the vicinity of the shock was approximately twice the value ahead of the shock. This peak additional heating appears to be sensitive to small variations in angle of sideslip.

Dryden Flight Research Facility
National Aeronautics and Space Administration
Edwards, California, November 1, 1990

APPENDIX
TRAJECTORY DERIVATION

No onboard airdata measurements were taken during the Pegasus flight. Therefore, free-stream airdata quantities were determined postflight by a combination of inertial data from an onboard inertial navigation system (INS), ground-based radar, and atmospheric data from balloons, stratospheric charts, and climatological information. Time of launch is defined as the release from the B-52 carrier aircraft, which occurred at 12:10:15 Pacific daylight time on April 5, 1990. The Pegasus vehicle was launched from 36° north, 123° west, which is off the coast of Monterey, California.

Inertial Navigation System

The INS determined position, velocity, accelerations, Euler angles, and body angle rates. Because of a software error in the INS, the position and velocity data were incorrectly calculated and were therefore determined from ground-based radar. Vehicle attitude and angular rate data were obtained from the INS.

Ground-Based Radar

Eight separate radar installations tracked the Pegasus vehicle. Three sites were located at Vandenberg Air Force Base, two at Point Pillar (near San Francisco), one at Point Mugu Naval Air Station, one at San Nicolas Island, and one at Edwards Air Force Base, California. The data from each radar site were low-pass filtered to 0.25 Hz and processed to give a time history of the vehicle position relative to the center of the Earth. Radar refraction errors were corrected using a balloon-measured index of a refraction profile from each radar site. The best estimate of the vehicle's position was determined by a weighted least squares combination of the data from all the radar sites. Weights were chosen as the inverse of the variance of each radar site's unfiltered second difference of position data. The position data were then differentiated and low-pass filtered to 0.10 Hz to yield velocity in the local north, east, and down directions. Filtering was accomplished using second-order Butterworth filters. Filter effects carry over to the calculated trajectory and do not account for discontinuous effects at launch. Consequently, data at launch are adjusted to correct for filter effects. Since radar data were not recorded prior to launch time, the radar position data were preceded by INS position data to allow the filters to initialize.

Atmospheric Model

A model of the atmosphere that covered the entire first-stage flight from the time of launch up to Z = 276,067 ft was constructed using a variety of sources. This model contains, as a function of Z, geometric altitude minus pressure altitude, ambient temperature, T_∞, wind velocity, W, and horizontal pressure gradient. Rawindsonde balloon data from the area were used to analyze the meteorological patterns that provided estimates of the atmospheric conditions in the area up to 78,000 ft. Between 78,000 and 118,000 ft, data were blended from both the rawindsonde balloons and the National Weather Service (NWS) stratospheric charts (for the location and day of launch). The NWS chart data were used exclusively from 118,000 to 180,000 ft where a transition was initiated to Pacific Missile Range April climatological data at altitudes above 200,000 ft (see ref. 2). In addition to this data, 10 min prior to launch the B-52 carrier and F-18 chase aircraft data were used to give an independent check of the pressure altitude, ambient temperature, and wind at the launch area.

Calculated Trajectory

The airdata state of the vehicle was calculated by using the inertial and atmospheric data. The time history of the pressure altitude of the Pegasus vehicle is shown in figure 7(a).

Airspeed is calculated by the difference between the inertial velocity and the wind velocity. Since the inertial velocity and wind velocity are in the local Earth north, east, down coordinate system, they were translated through the roll, pitch, and yaw angles, (ϕ, θ, Ψ), of the Pegasus vehicle to give the body axes airspeed components, u, v, and w by the following transformation operation:

$$\begin{bmatrix} u \\ v \\ w \end{bmatrix} = \Gamma \left\{ \begin{bmatrix} V_N \\ V_E \\ V_D \end{bmatrix} - \begin{bmatrix} W_N \\ W_E \\ 0 \end{bmatrix} \right\}$$

where

$$\Gamma = \begin{bmatrix} 1 & 0 & 0 \\ 0 & \cos(\phi) & \sin(\phi) \\ 0 & -\sin(\phi) & \cos(\phi) \end{bmatrix} \begin{bmatrix} \cos(\theta) & 0 & -\sin(\theta) \\ 0 & 1 & 0 \\ \sin(\theta) & 0 & \cos(\theta) \end{bmatrix} \begin{bmatrix} \cos(\Psi) & \sin(\Psi) & 0 \\ -\sin(\Psi) & \cos(\Psi) & 0 \\ 0 & 0 & 1 \end{bmatrix}$$

The total free-stream airspeed is

$$V_\infty = \sqrt{u^2 + v^2 + w^2}$$

The free-stream velocity and the ambient temperature obtained from the atmospheric model are used with the ideal gas constant, R, ratio of specific heats of air, γ, and the acceleration of gravity at sea level, g, to give free-stream Mach number

$$M_\infty = \frac{V_\infty}{\sqrt{\gamma R g T_\infty}}$$

which is shown in figure 7(b). Note that the vehicle attained Mach numbers in excess of Mach 8.0 before first-stage separation.

Free-stream static pressure, Ps_∞, is determined from pressure altitude, and ambient atmospheric density, ρ_∞, is calculated by

$$\rho_\infty = \frac{Ps_\infty}{R T_\infty}$$

and dynamic pressure, $\bar{q}$, is given by

$$\bar{q} = \frac{\rho_\infty}{2\,g} V_\infty^2$$

which is shown in figure 7(c).

Now true angle of attack and angle of sideslip may be determined from the airspeed components by

$$\alpha = \tan^{-1}\left[\frac{w}{u}\right]$$

$$\beta = \sin^{-1}\left[\frac{v}{V_\infty}\right]$$

shown in figures 7(d) and (e), respectively.

REFERENCES

1. Mendenhall, Michael R., Daniel J. Lesieutre, Steven C. Caruso, Marnix F.E. Dillenius, and Gary D. Kuhn, "Aerodynamic Design of Pegasus™: Concept to Flight with CFD," *Missile Aerodynamics*, AGARD-CP-493, 1990.

2. White Sands Missile Range, *Pacific Missile Test Center Reference Atmosphere for Point Arguello, California Part 2*, IRIG Document 104-63, Nov. 1975.

3. Hartung, Lin C., and David A. Throckmorton, *Space Shuttle Entry Heating Data Book, Volume 1–STS-2*, NASA RP-1191, part 1, 1988.

4. Ames Research Staff, "Equations, Tables and Charts for Compressible Flow," *Thirty-Ninth Annual Report of the National Advisory Committee for Aeronautics*, NACA Report 1135, 1953, pp. 613–681.

5. Carslaw, H.S., and J.C. Jaeger, *Conduction of Heat in Solids*, Second ed., Oxford University Press, 1959.

6. Holman, J.P., *Heat Transfer*, Fifth ed., McGraw-Hill Book Co., 1981.

7. Hankey, Wilbur L. Jr., 1st Lt. Richard D. Neumann, and Evard H. Flinn, *Design Procedures for Computing Aerodynamic Heating at Hypersonic Speeds*, WADC Technical Report 59-610, June 1960.

Table 1. Properties of TPS materials.

Material	ρ, lb_m in^{-3}	k, Btu in^{-1} sec^{-1} $°F^{-1}$	C_p, Btu lb_m^{-1} $°F^{-1}$	$Heat_{abl}$, Btu lb_m^{-1}	T_{act}, °F	T_{alb}, °F	Description
Insulator	0.00613	0.598×10^{-6}	0.262	n/a	n/a	n/a	Patterned after insulator on shuttle main tank. Microballoons in epoxy. Spray-on application.
Cork	0.0177	0.925×10^{-6}	0.47	n/a	n/a	n/a	Multipurpose insulator. Organic fiber. Bonded in place.
Firex	0.04	3.24×10^{-6}	0.4	1800	280	250	Low-temperature ablative material. Polymer. Spray-on application.
Thermolag	0.0521	1.85×10^{-6}	0.3	750	n/a	230	Low-temperature ablative material. Polymer. Spray-on application.

Table 2. Sensor distribution.

	Foil gages	Bulb gages	HRSI plugs
Wing upper surface	3	2	0
Wing lower surface	25	6	0
Leading edge	15	0	0
Fillet	18	2	10
Signal conditioning equipment	0	5	0
Total	61	15	10

Table 3. HRSI material properties; HRSI density (LI-2200) = 22 lb_m ft^{-3}.

(a) Thermal conductivity.

	Pressure, atmosphere					
Temperature, °F	10^{-5}	10^{-4}	10^{-3}	10^{-2}	10^{-1}	1
−250	0.0133	0.0133	0.0167	0.0267	0.0300	0.0333
−150	0.0150	0.0150	0.0183	0.0283	0.0333	0.0367
75	0.0183	0.0183	0.0233	0.0333	0.0408	0.0467
500	0.0250	0.0250	0.0317	0.0408	0.0558	0.0650
1000	0.0358	0.0358	0.0442	0.0533	0.0783	0.0900
1500	0.0500	0.0500	0.0600	0.0708	0.1058	0.1192
1700	0.0583	0.0583	0.0683	0.0808	0.1192	0.1342
2000	0.0692	0.0692	0.0833	0.0983	0.1417	0.1583
2300	0.0842	0.0842	0.1000	0.1200	0.1658	0.1883

(b) Specific heat.

Temperature, °F	C_p, Btu lb_m^{-1} $°F^{-1}$
−250	0.070
−150	0.105
0	0.150
250	0.210
500	0.252
750	0.275
1000	0.288
1250	0.296
1500	0.300
1700	0.302
1750	0.303
3000	0.303

Table 4. Roll-off frequencies used in postflight filtering.

Channel, FS, in.; z, in.	Roll-off frequency of filter, ω
FS = 246.2, z = 23	4
FS = 253.1, z = 23	4
FS = 280.6, z = 23	2.5
FS = 288.4, z = 23	2.5
FS = 253.1, z = 18	2.86
FS = 280.6, z = 17	4
FS = 288.4, z = 17	2.5
FS = 241.0, z = 11	2.5
FS = 253.1, z = 11	2
FS = 280.6, z = 11	2.5

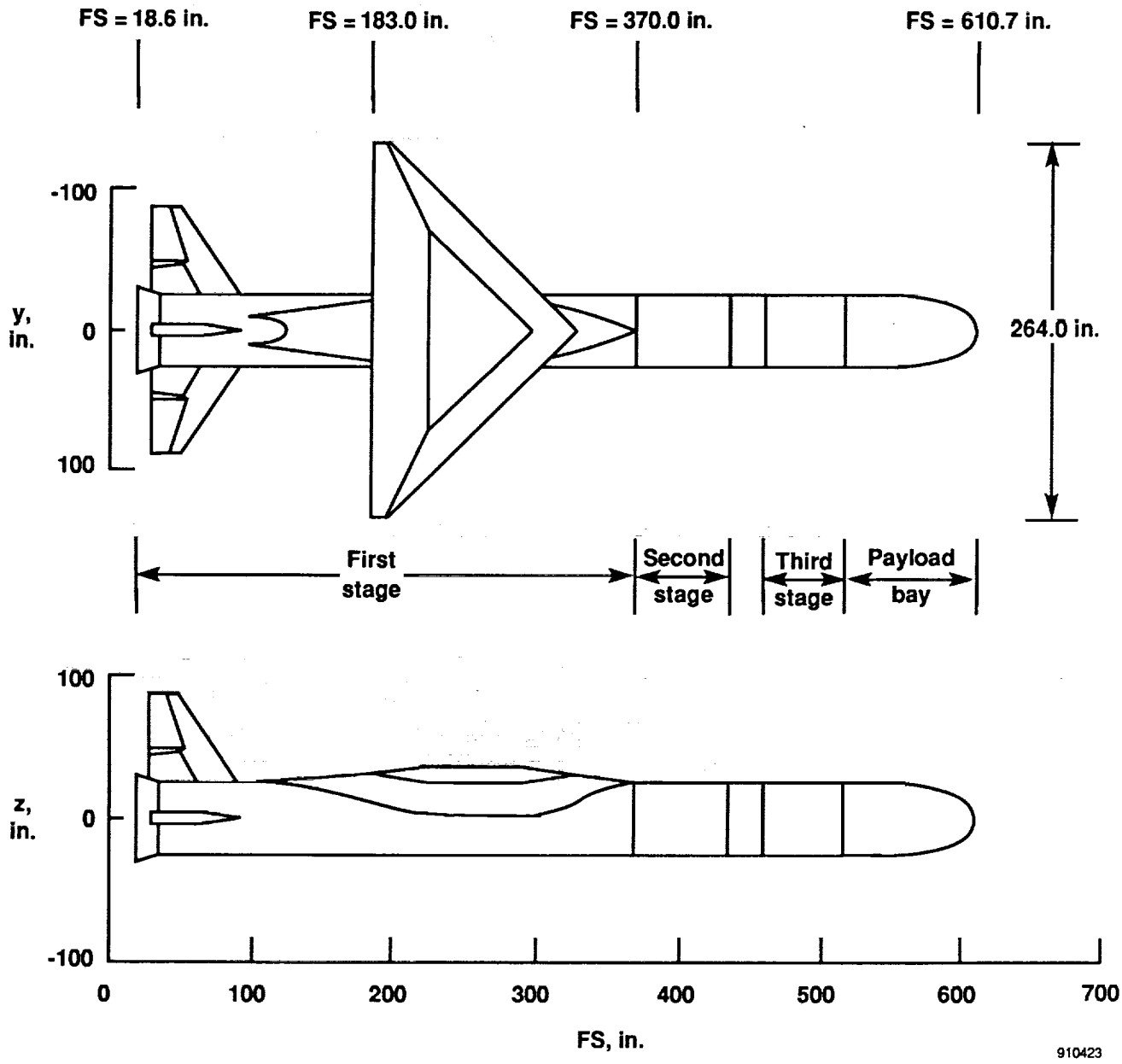

(a) Pegasus two-view.

Figure 1. Pegasus launch configuration.

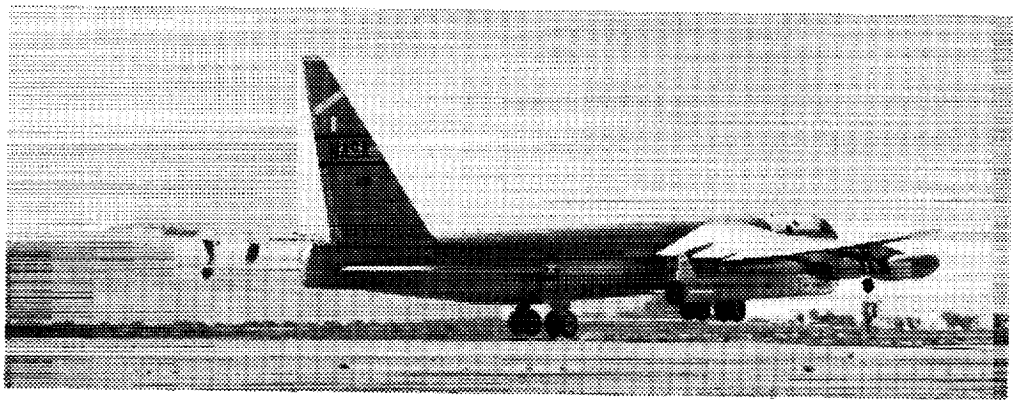

EC90 111-1

(b) B-52 carrier and Pegasus vehicle at takeoff.

Figure 1. Concluded.

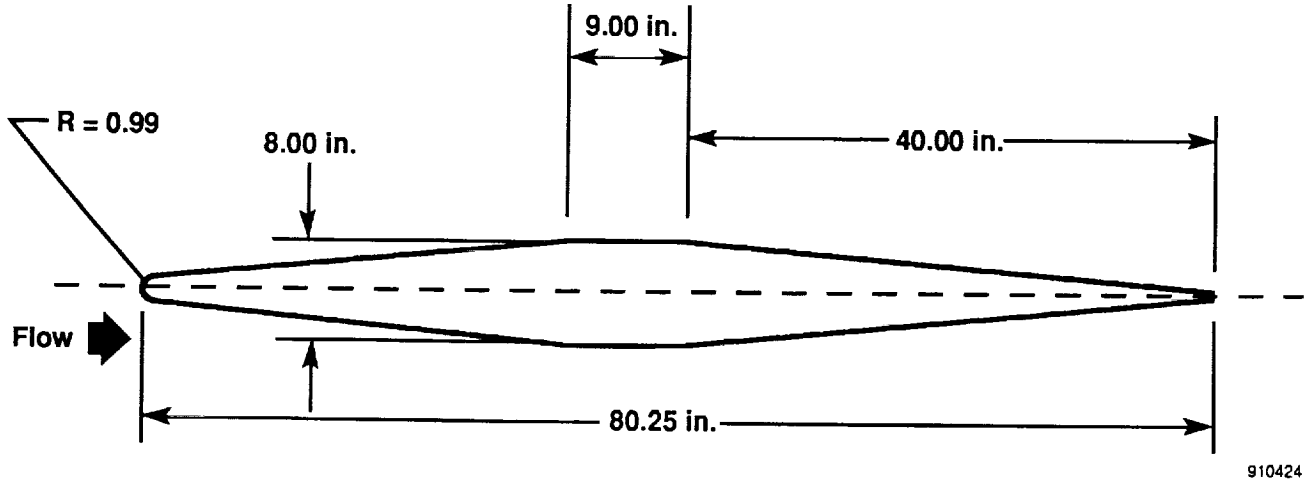

(a) Airfoil section at y = 65 in.

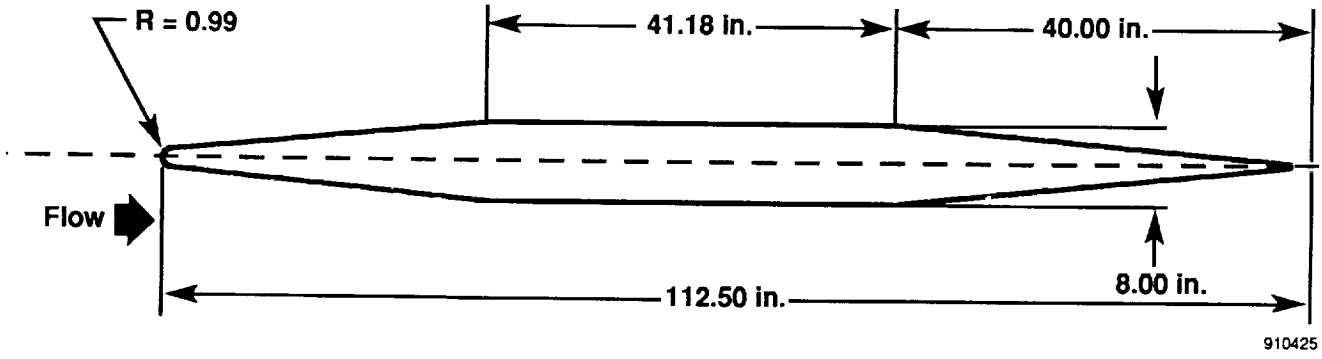

(b) Airfoil section at y = 32 in.

Figure 2. Airfoil section diagrams.

ORIGINAL PAGE
BLACK AND WHITE PHOTOGRAPH

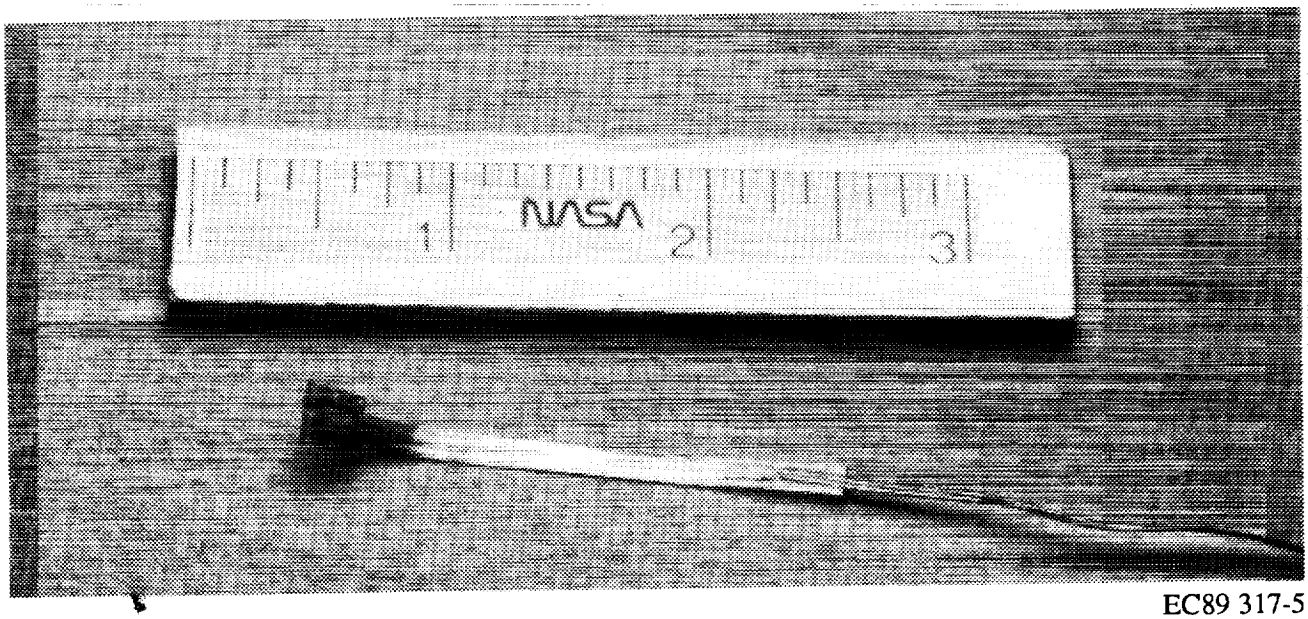

EC89 317-5

Figure 3. Foil TC sensor and leads.

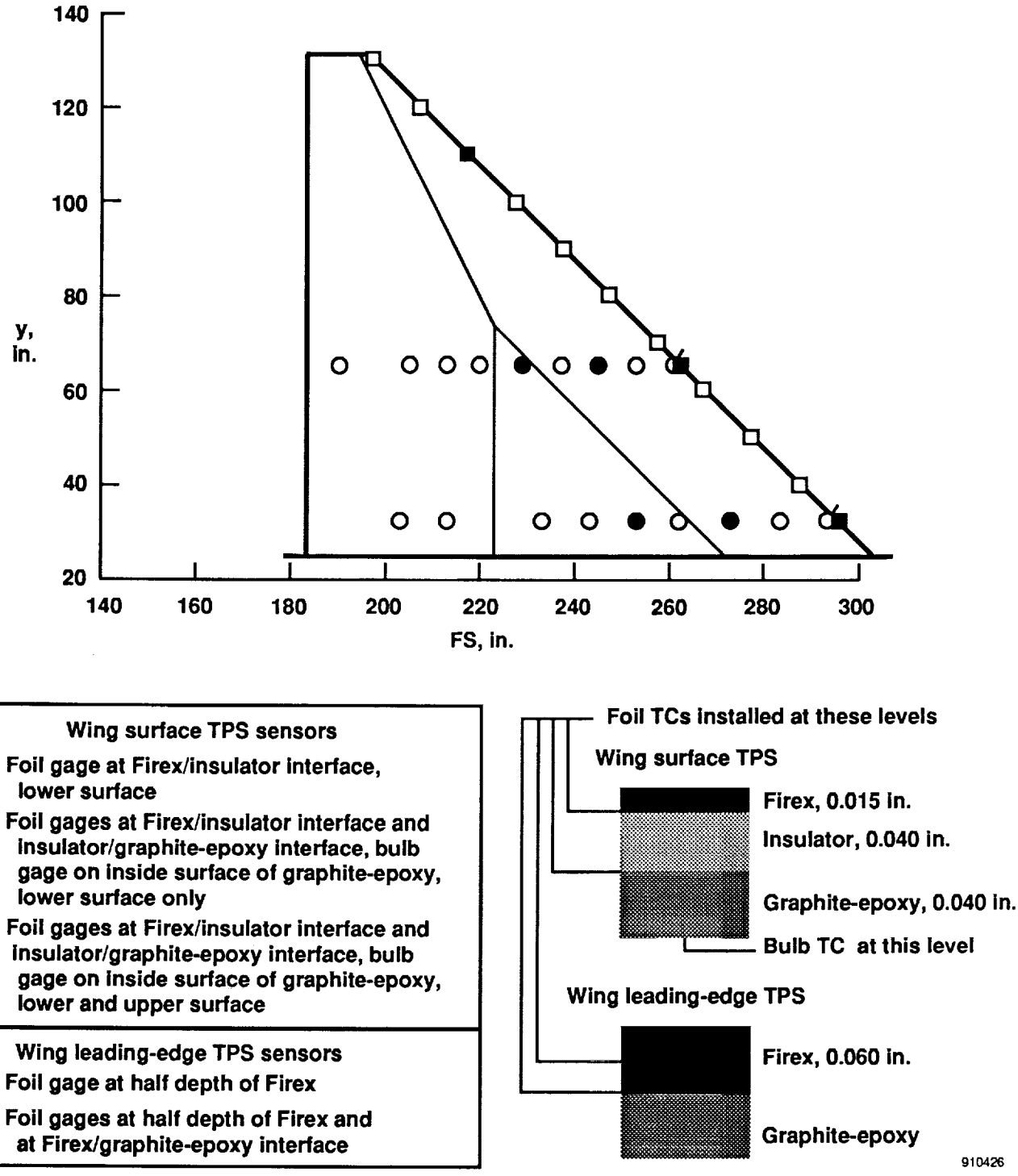

Figure 4. Plan view of wing lower surface, showing sensor locations.

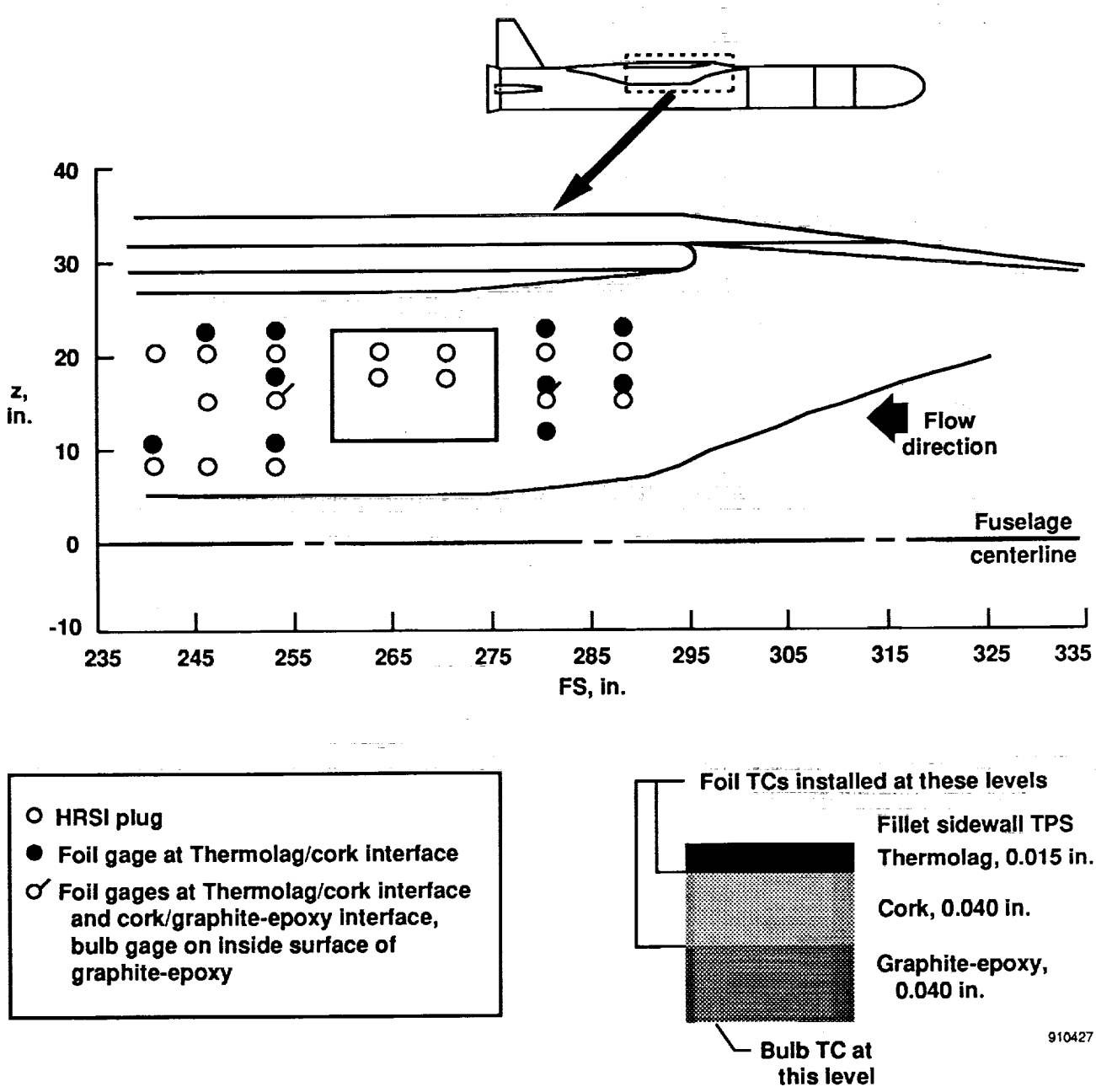

Figure 5. Side view of wing-body fillet, showing sensor locations.

ORIGINAL PAGE
BLACK AND WHITE PHOTOGRAPH

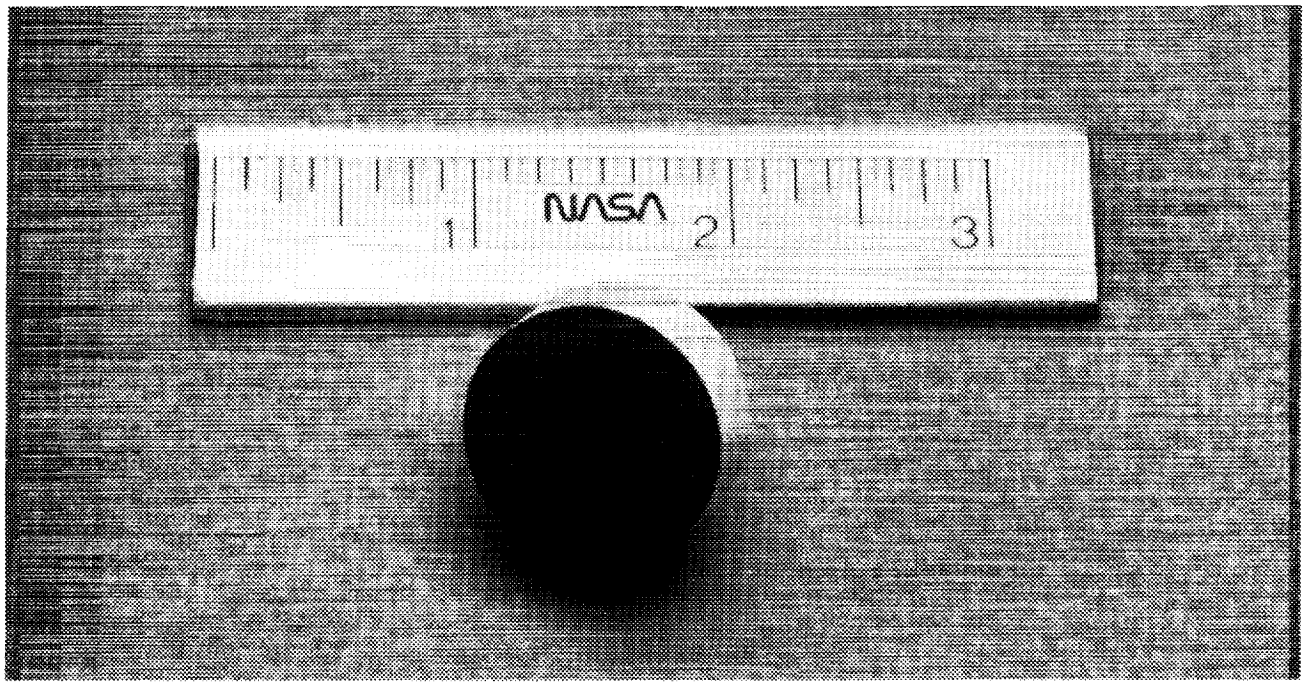

EC89 0317-003

(a) HRSI plug.

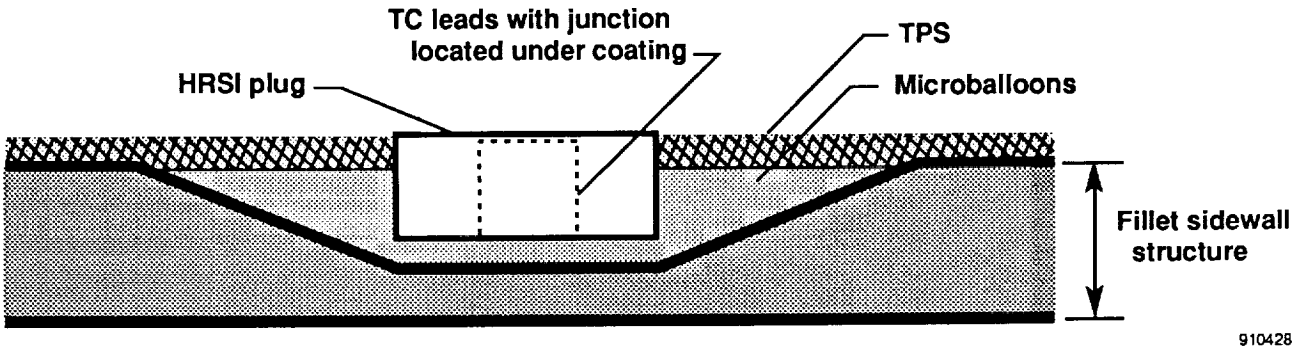

(b) Cross-sectional diagram of HRSI plug installation.

Figure 6. HRSI plug illustrations.

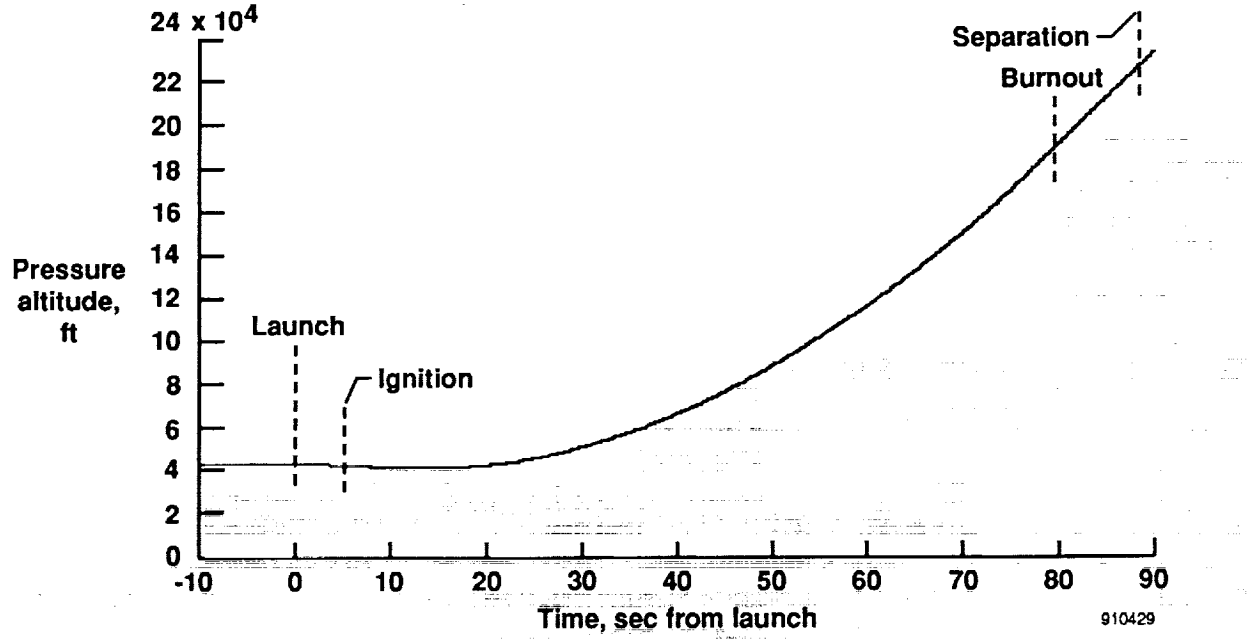

(a) Pressure altitude.

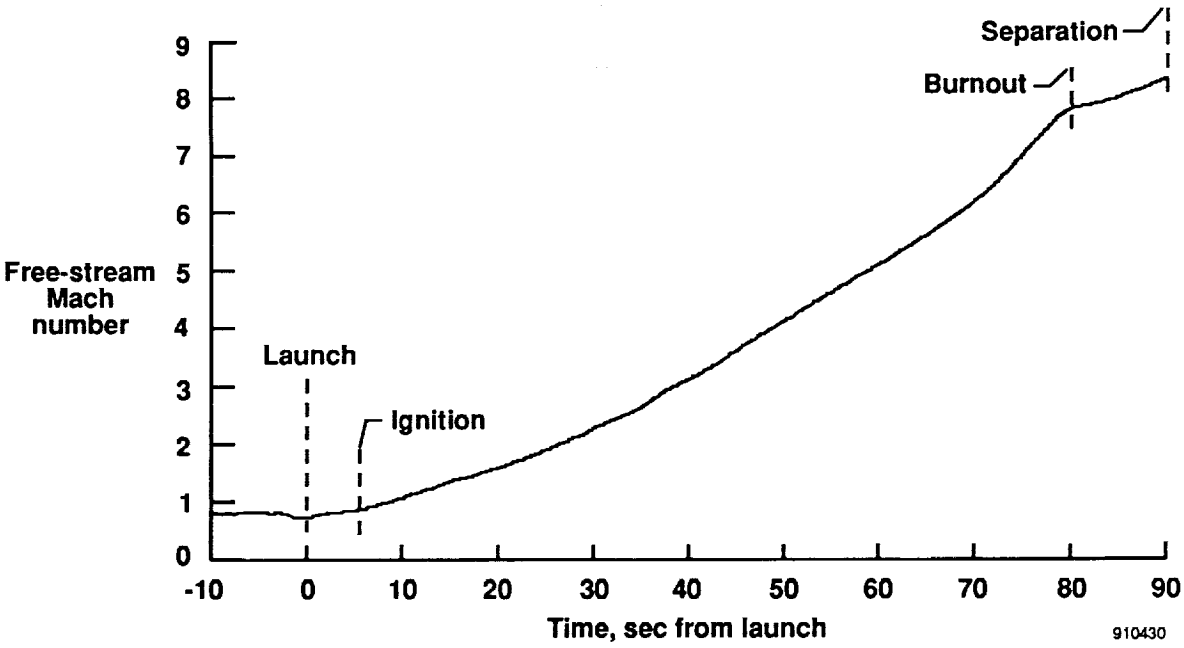

(b) Free-stream Mach number.

Figure 7. Trajectory time histories.

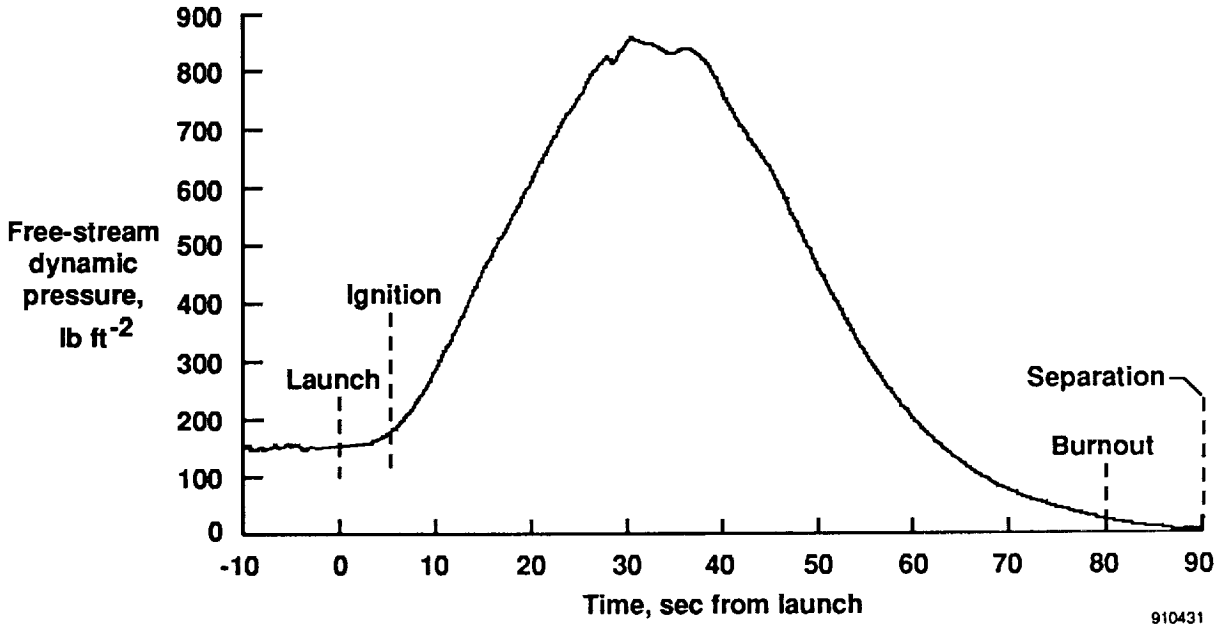

(c) Free-stream dynamic pressure.

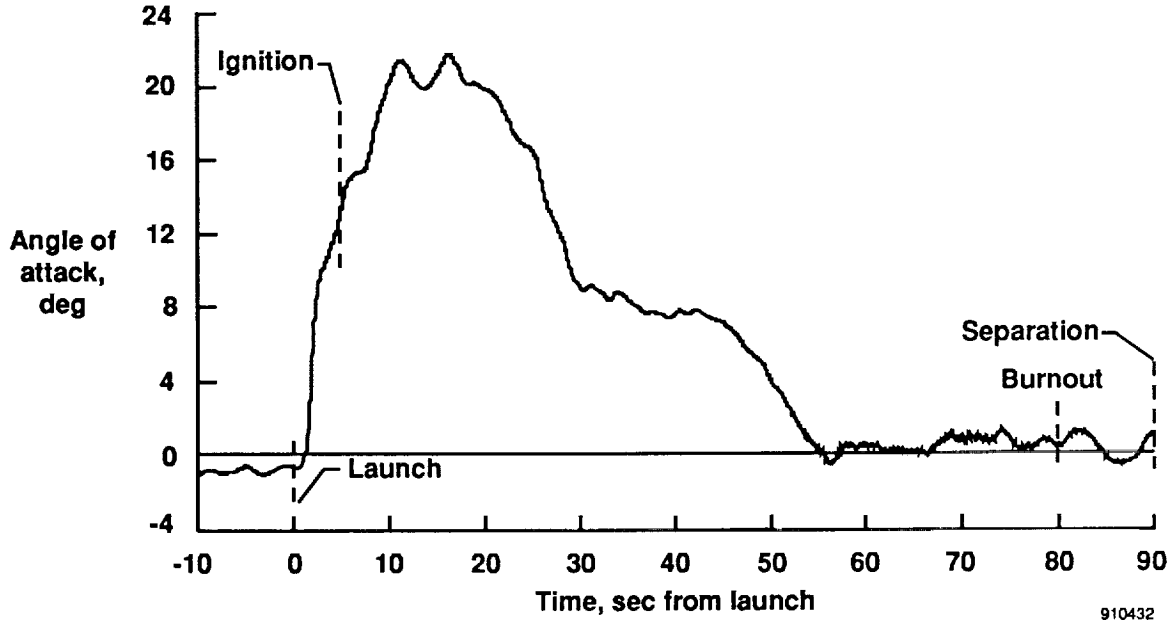

(d) Angle of attack.

Figure 7. Continued.

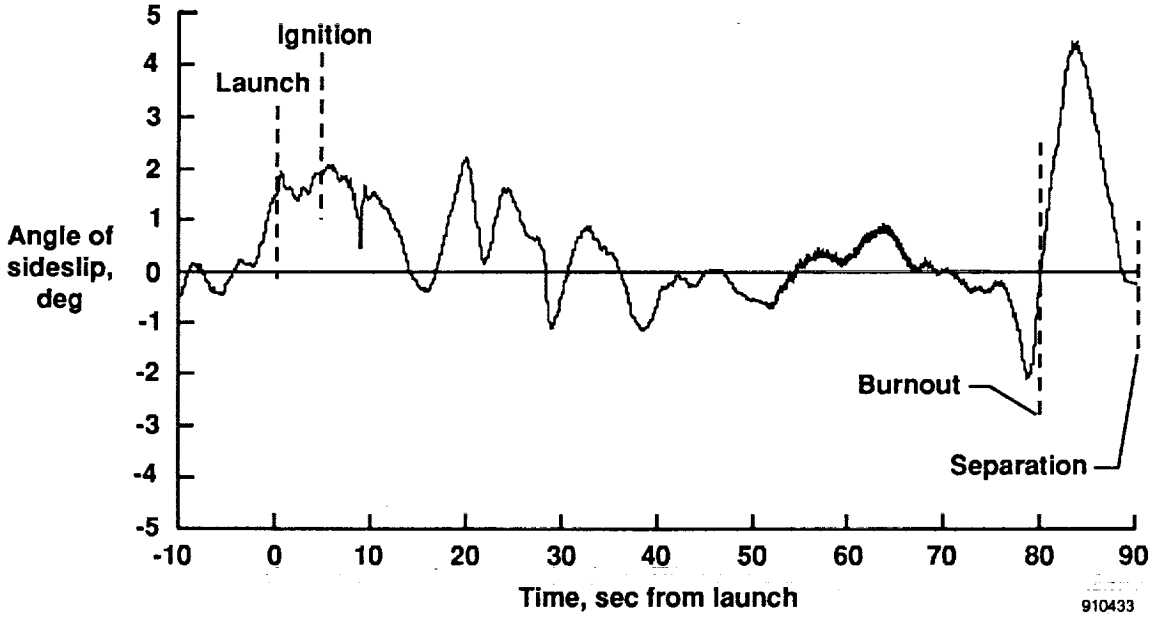

(e) Angle of sideslip.

Figure 7. Concluded.

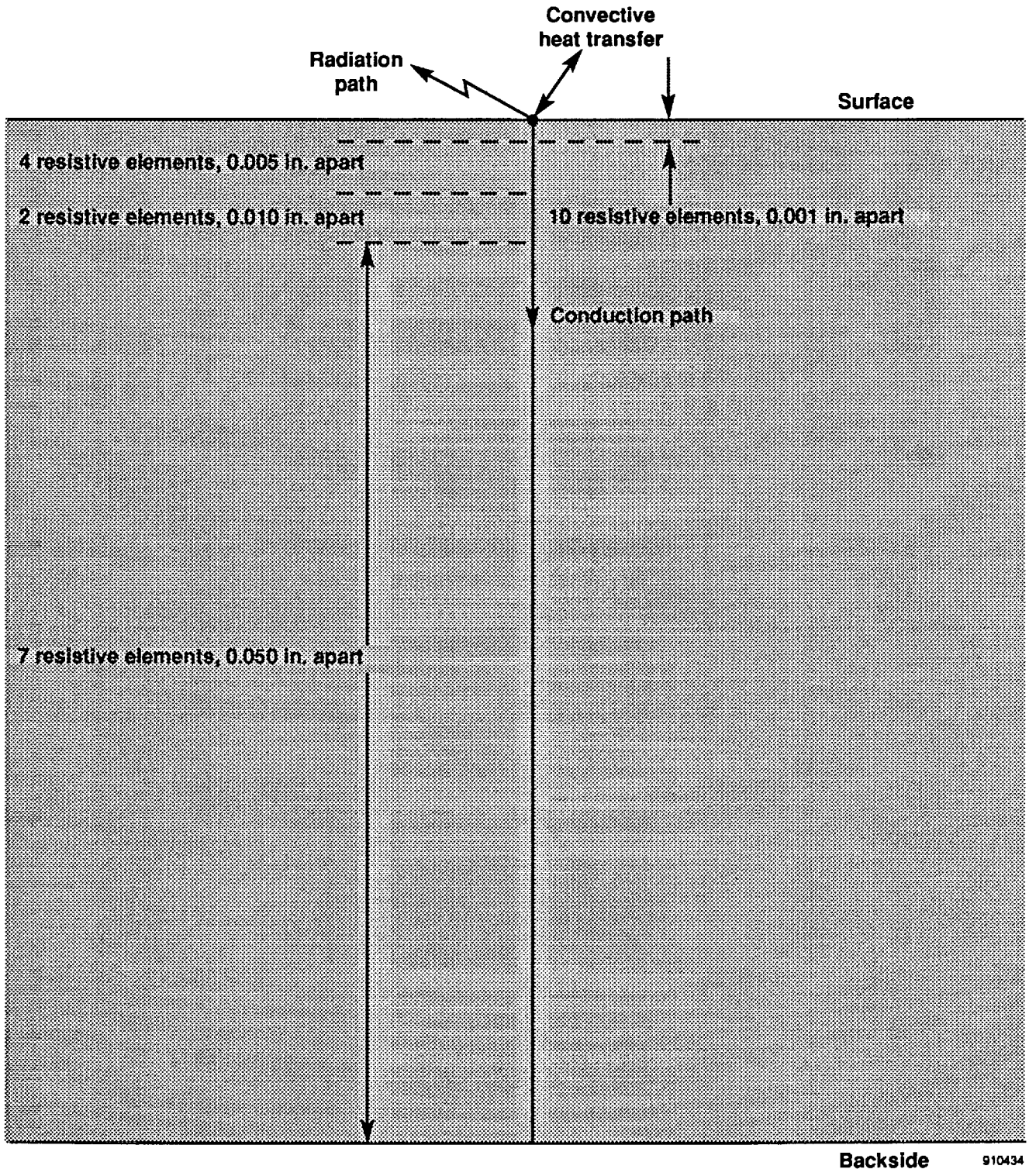

Figure 8. LTA model of HRSI plug.

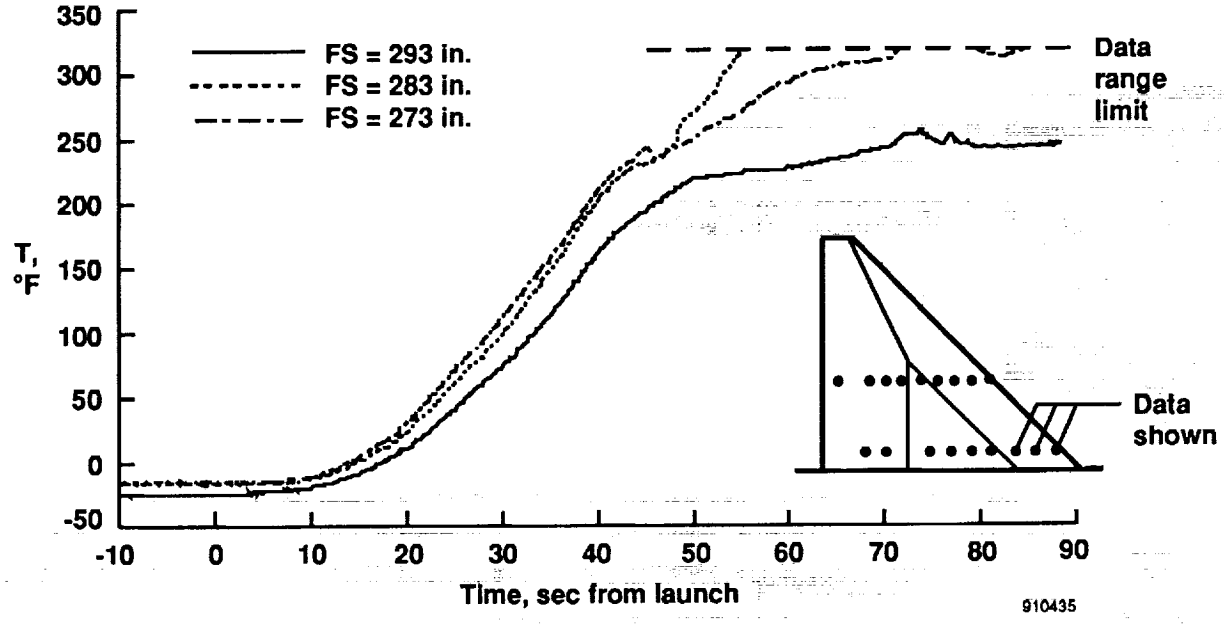

(a) FS = 293, 283, and 273 in.

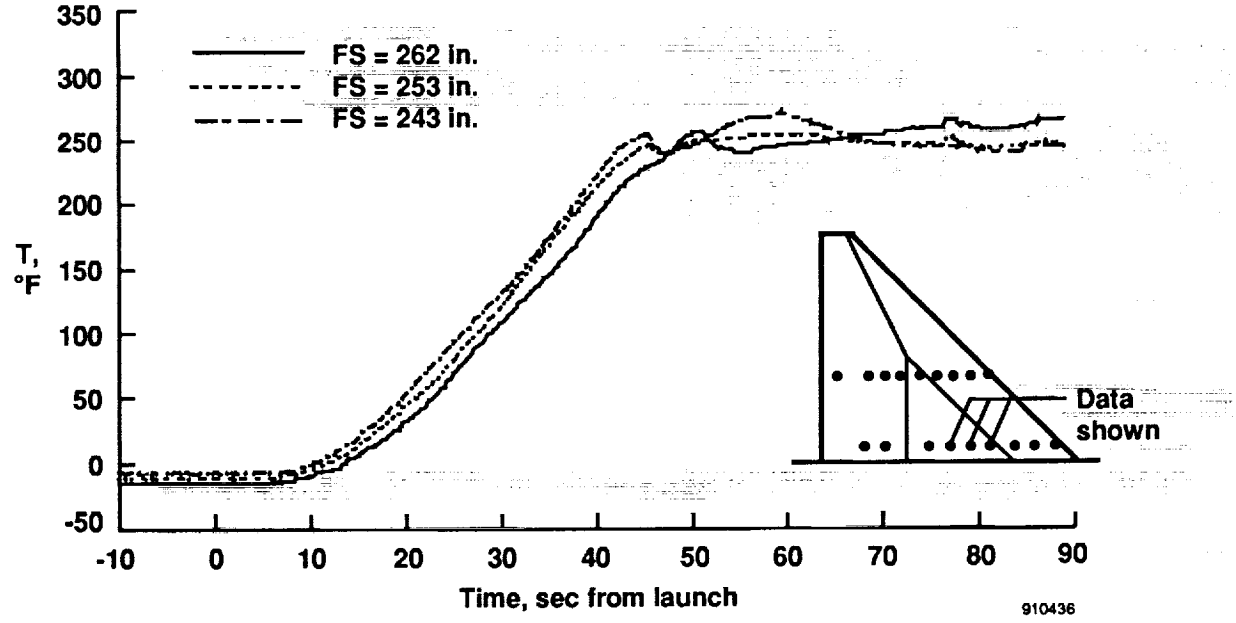

(b) FS = 262, 253, and 243 in.

Figure 9. Lower surface wing temperatures, inboard row (y = 32 in.), Firex–insulator interface, °F.

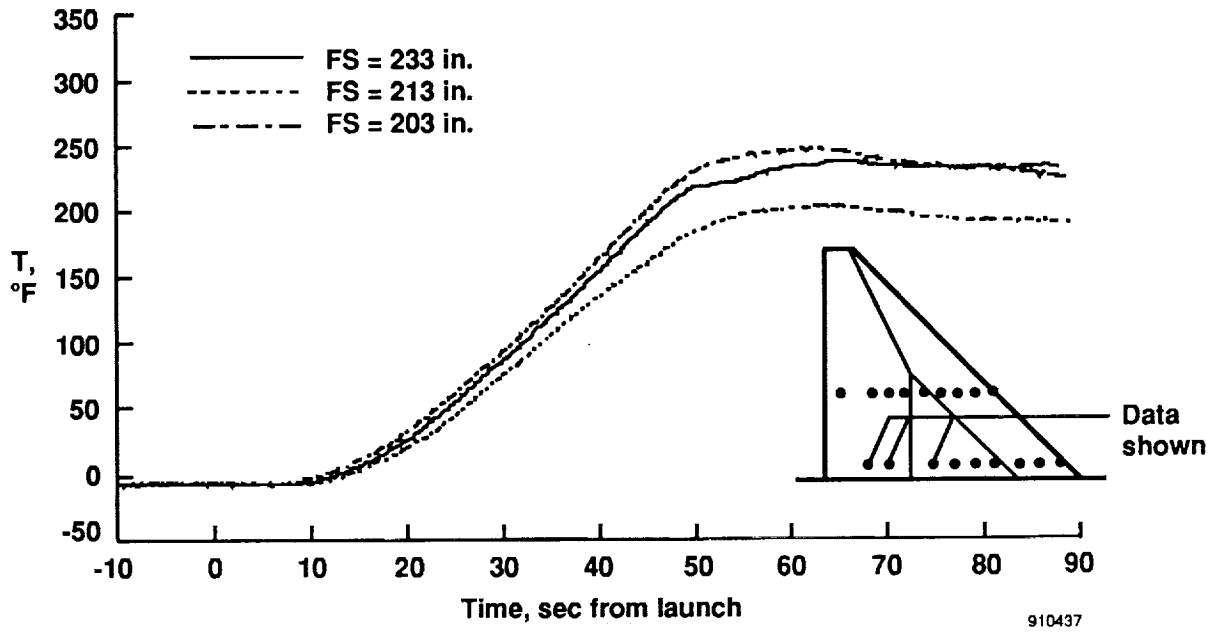

(c) FS = 233, 213, and 203 in.

Figure 9. Concluded.

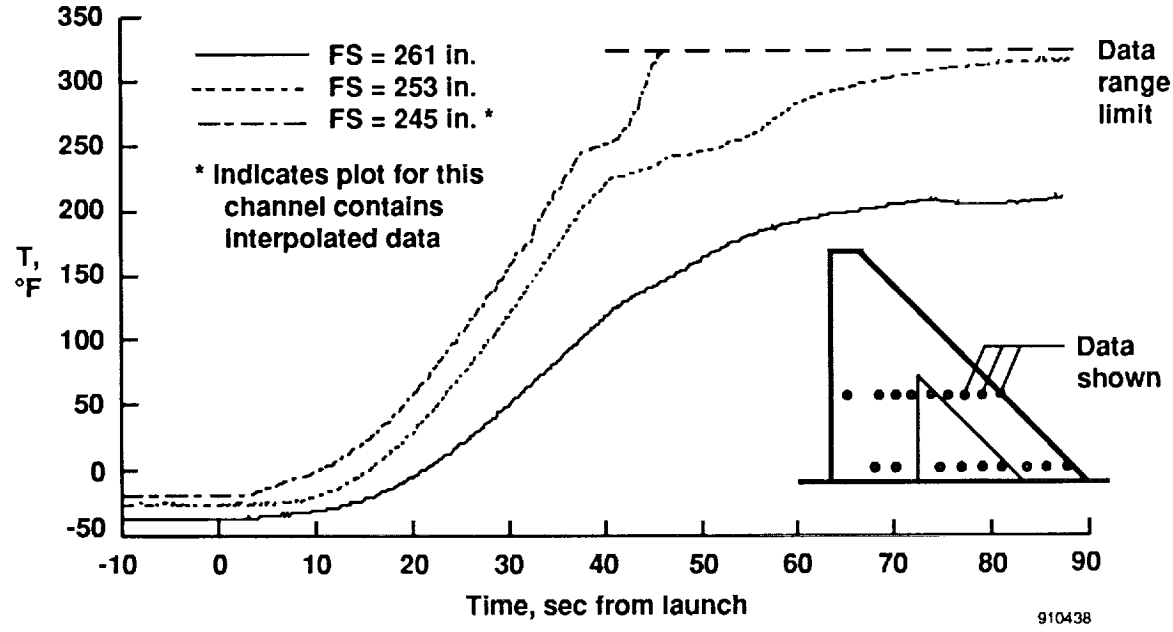

(a) FS = 261, 253, and 245 in.

Figure 10. Lower surface wing temperatures, outboard row (y = 65 in.), Firex–insulator interface, °F.

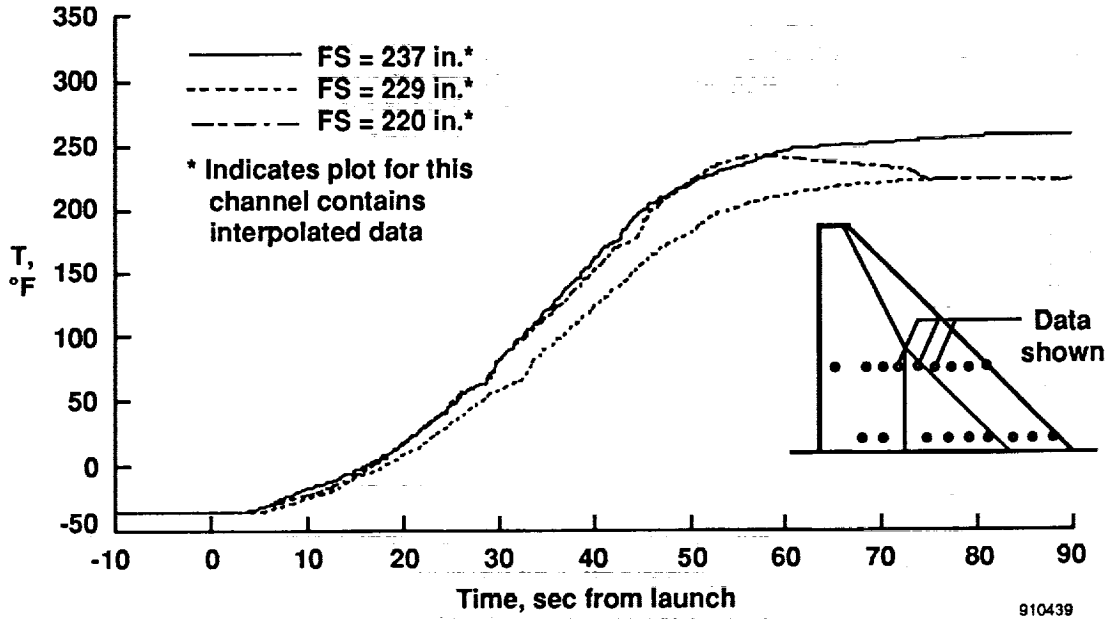

(b) FS = 237, 229, and 220 in.

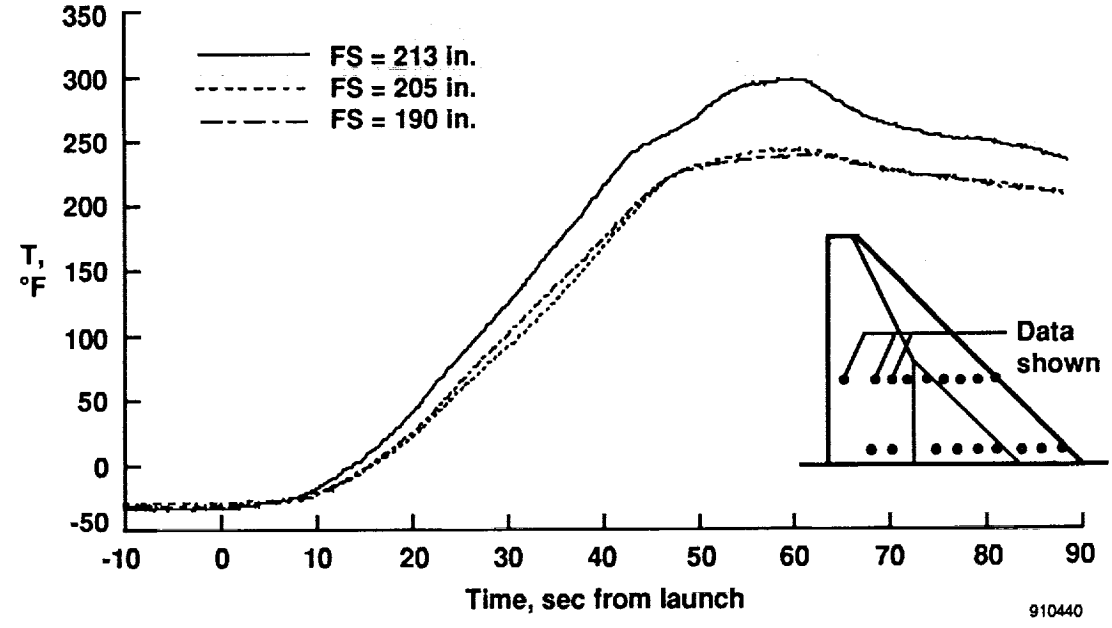

(c) FS = 213, 205, and 190 in.

Figure 10. Concluded.

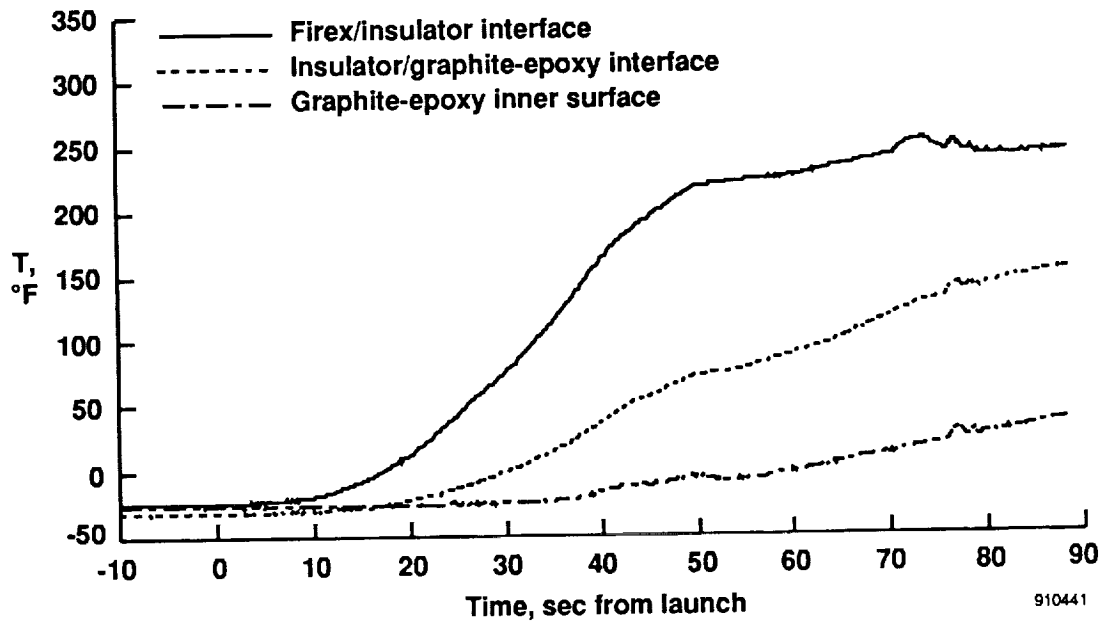

(a) FS = 293 in., y = 32 in.

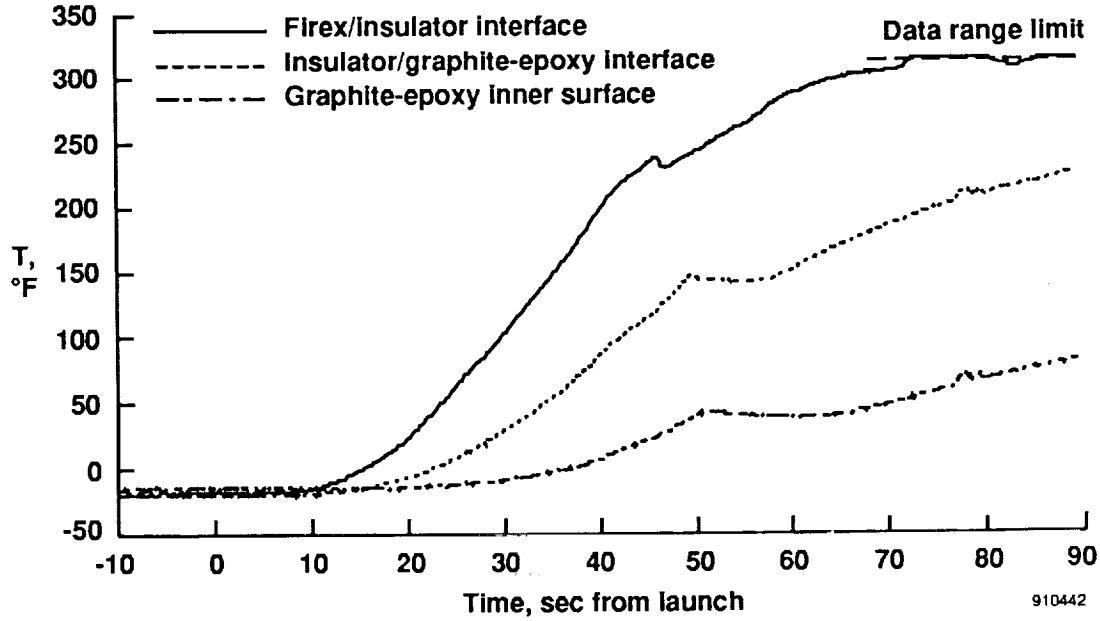

(b) FS = 273 in., y = 32 in.

Figure 11. Wing TPS interface temperatures, °F.

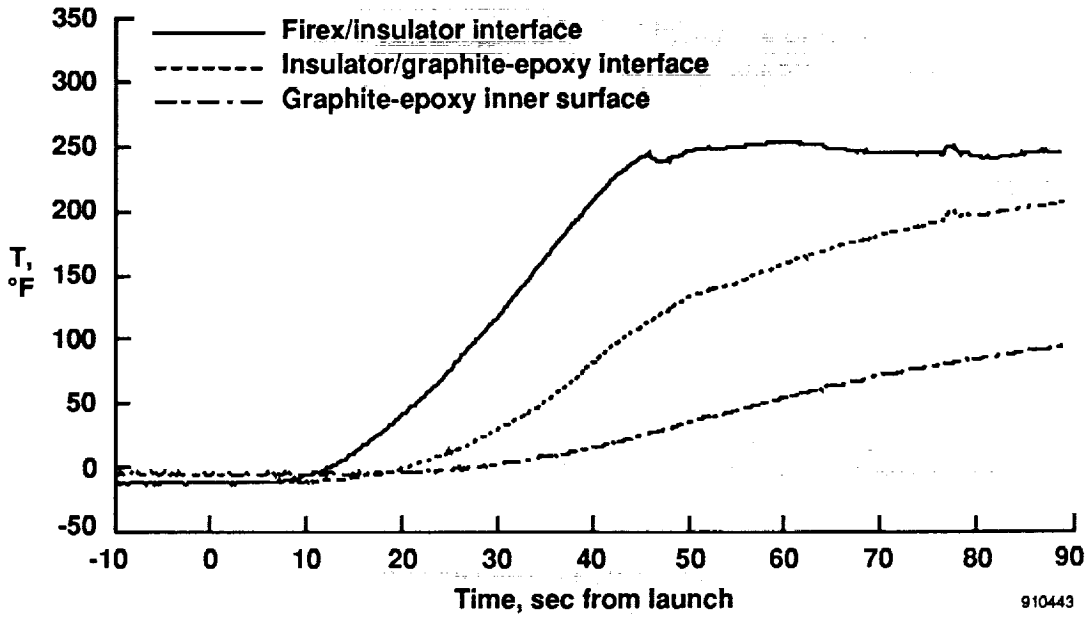

(c) FS = 253 in., y = 32 in.

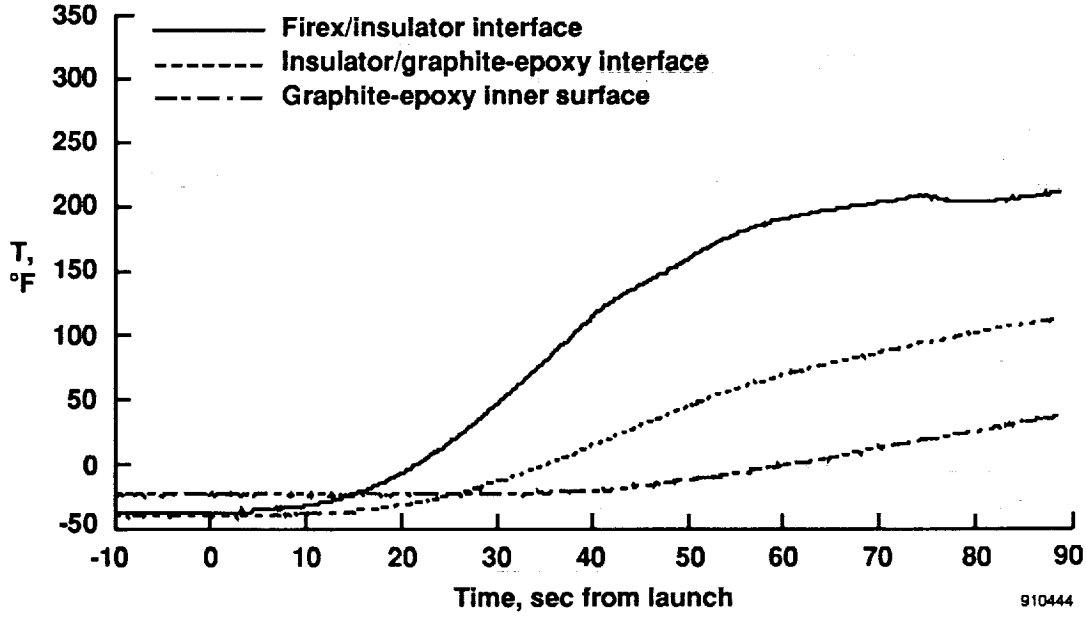

(d) FS = 261 in., y = 65 in.

Figure 11. Continued.

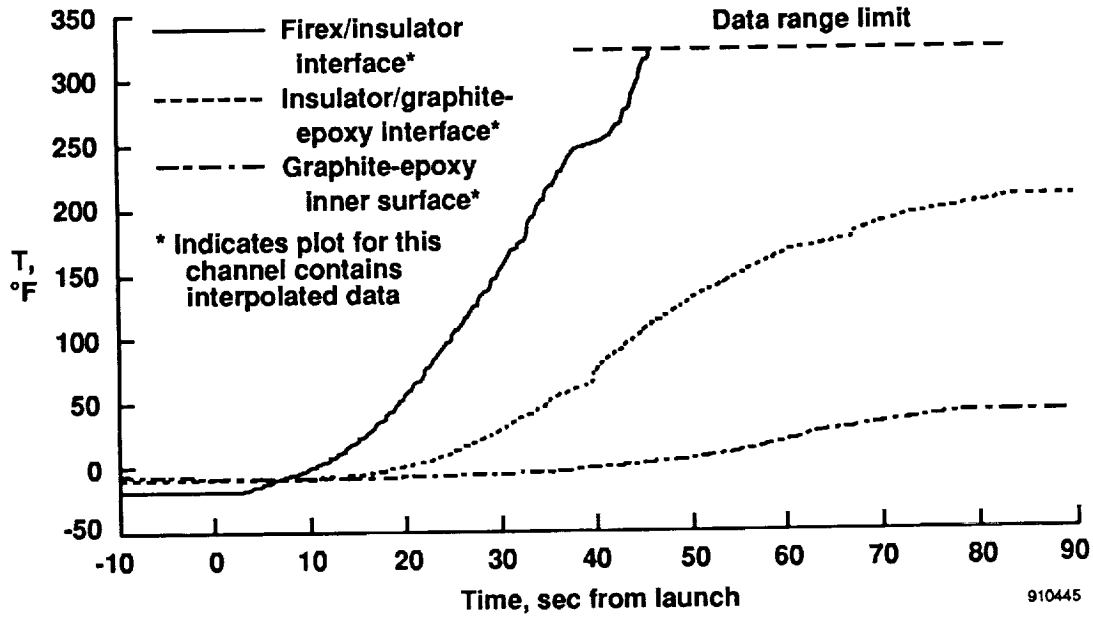

(e) FS = 245 in., y = 65 in.

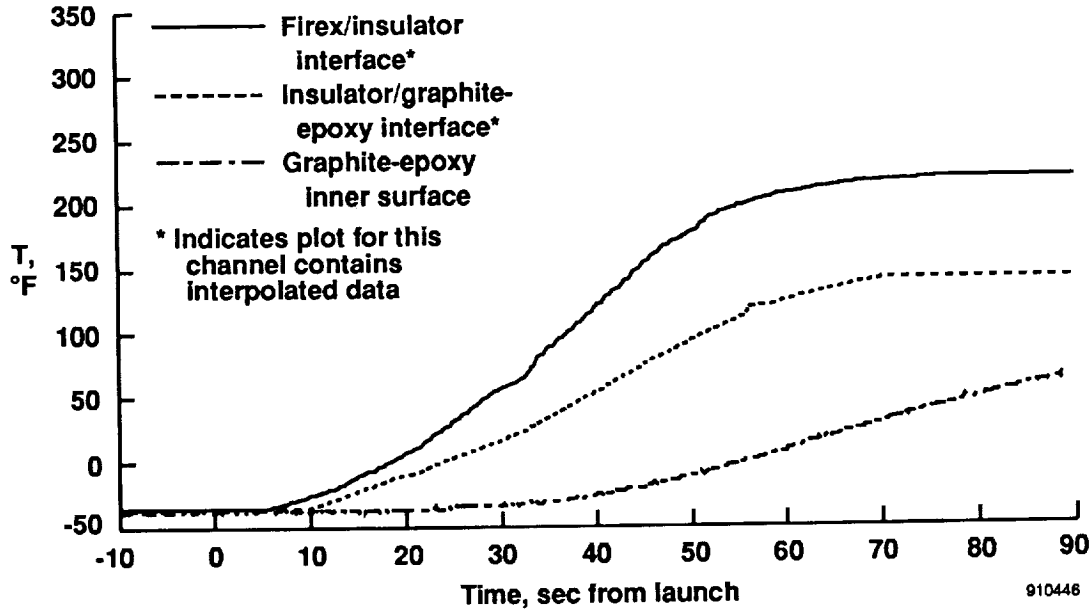

(f) FS = 229 in., y = 65 in.

Figure 11. Concluded.

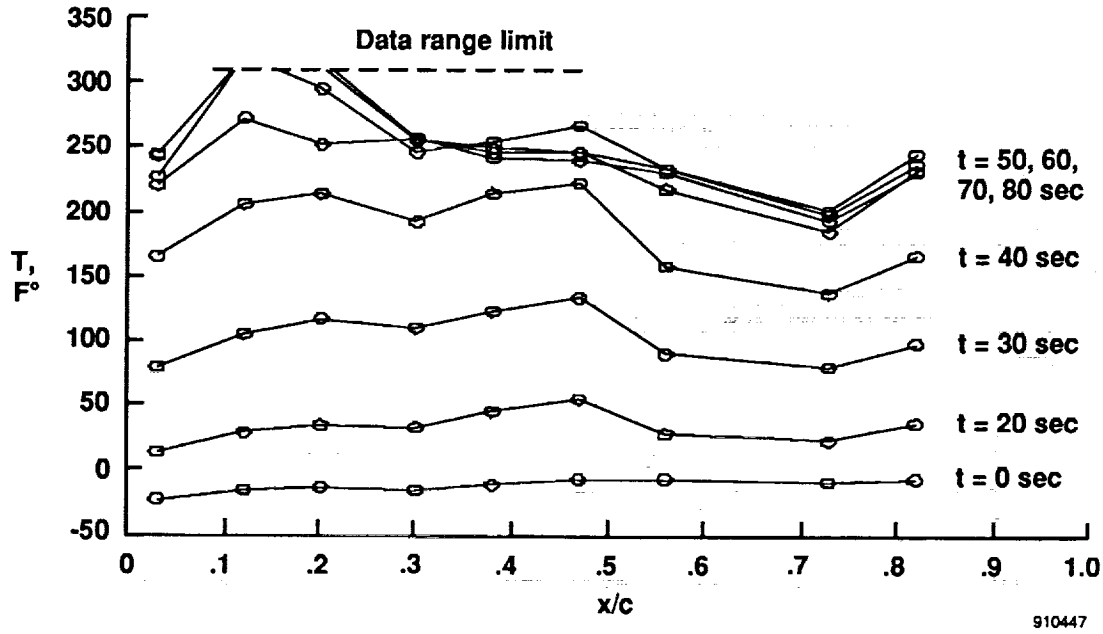

(a) Inboard row, y = 32 in.

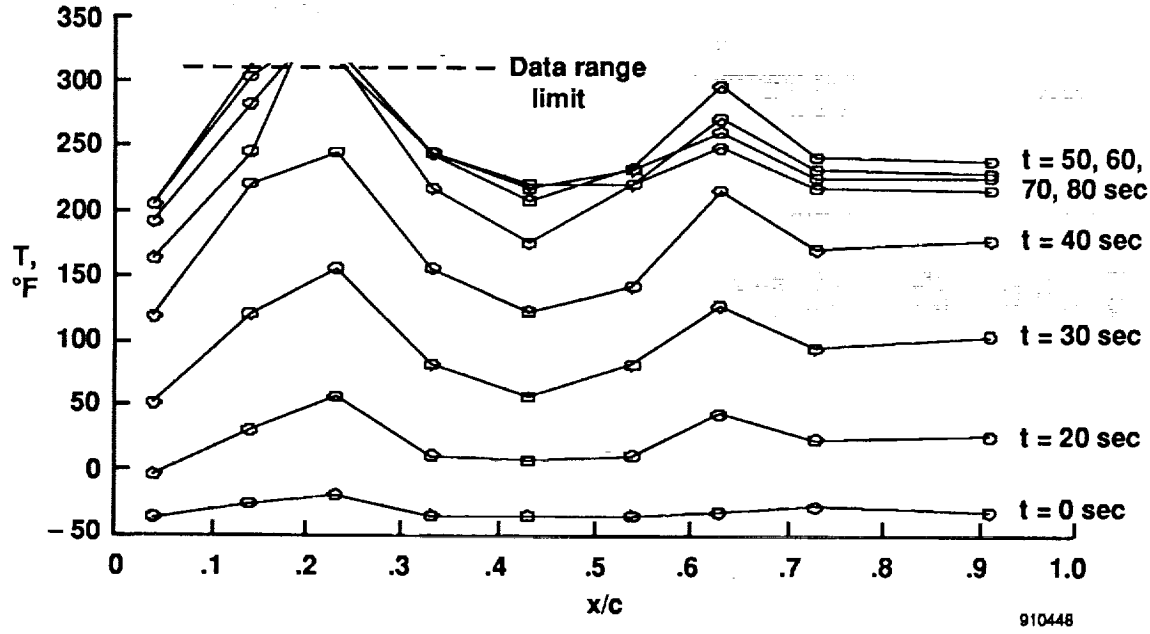

(b) Outboard row, y = 65 in.

Figure 12. Chordwise distribution of wing lower surface temperatures at the Firex–insulator interface, °F.

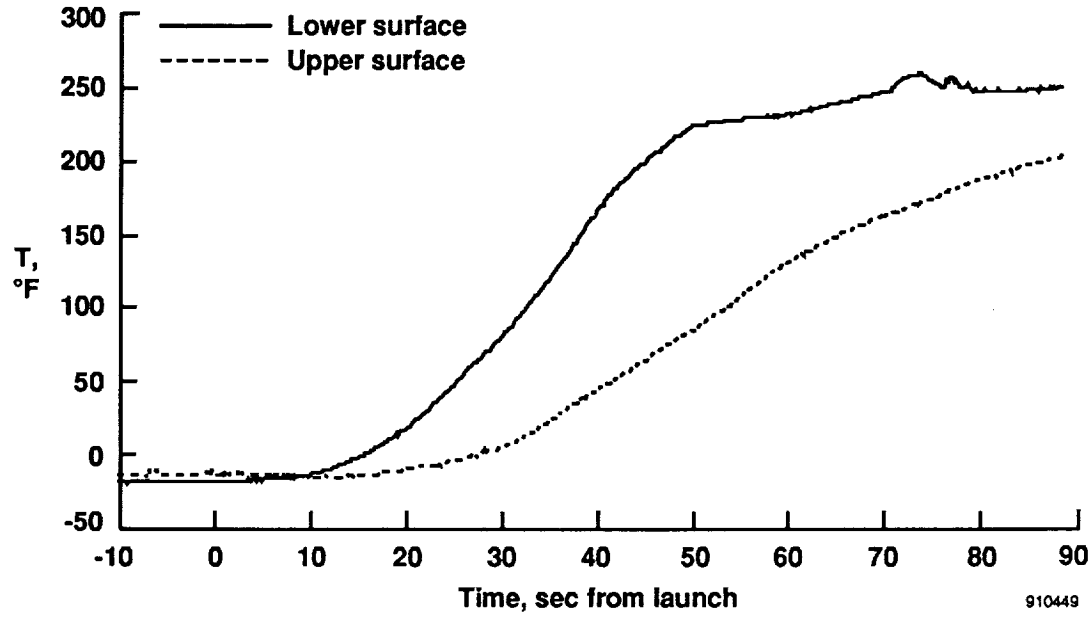

(a) FS = 283 in., y = 32 in.

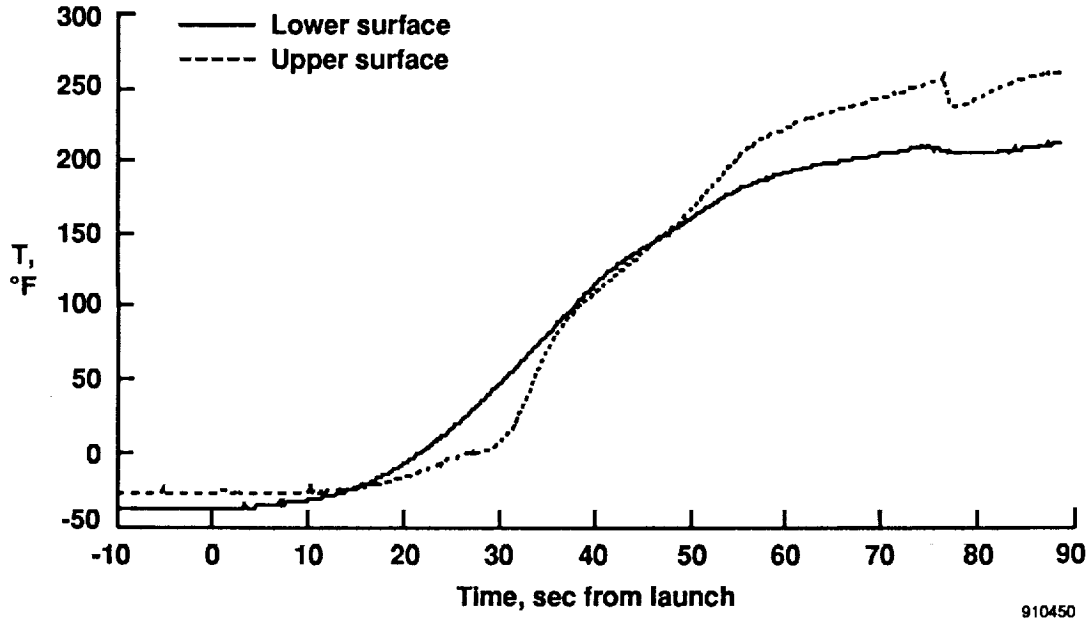

(b) FS = 261 in., y = 65 in.

Figure 13. Comparison of upper and lower surface wing temperatures at the Firex–insulator interface, °F.

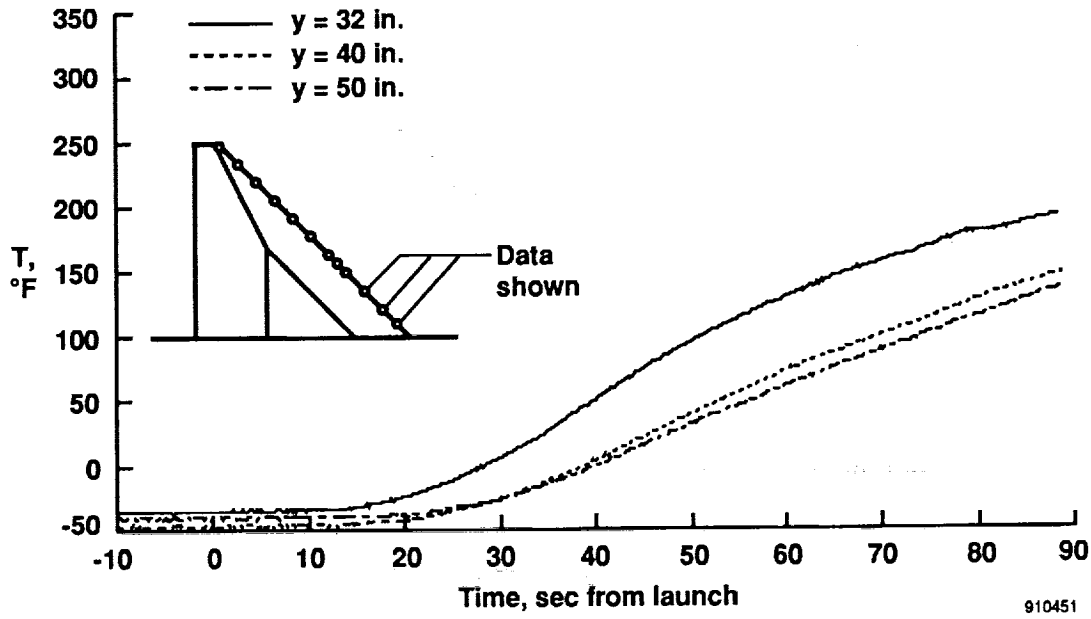

(a) y = 32, 40, and 50 in.

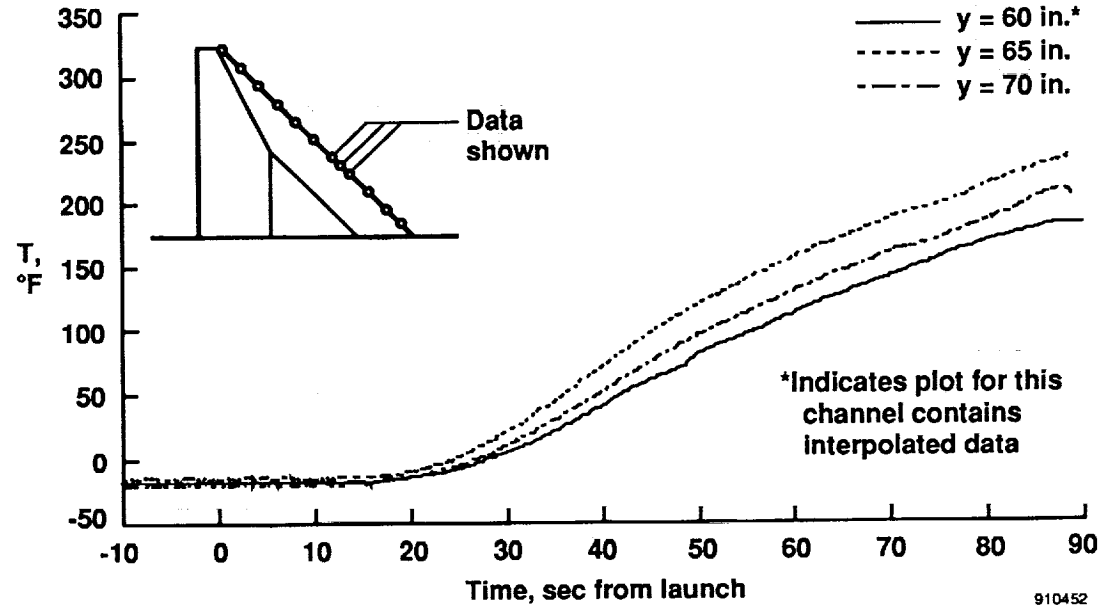

(b) y = 60, 65, and 70 in.

Figure 14. Wing leading-edge temperatures at half depth of Firex, °F.

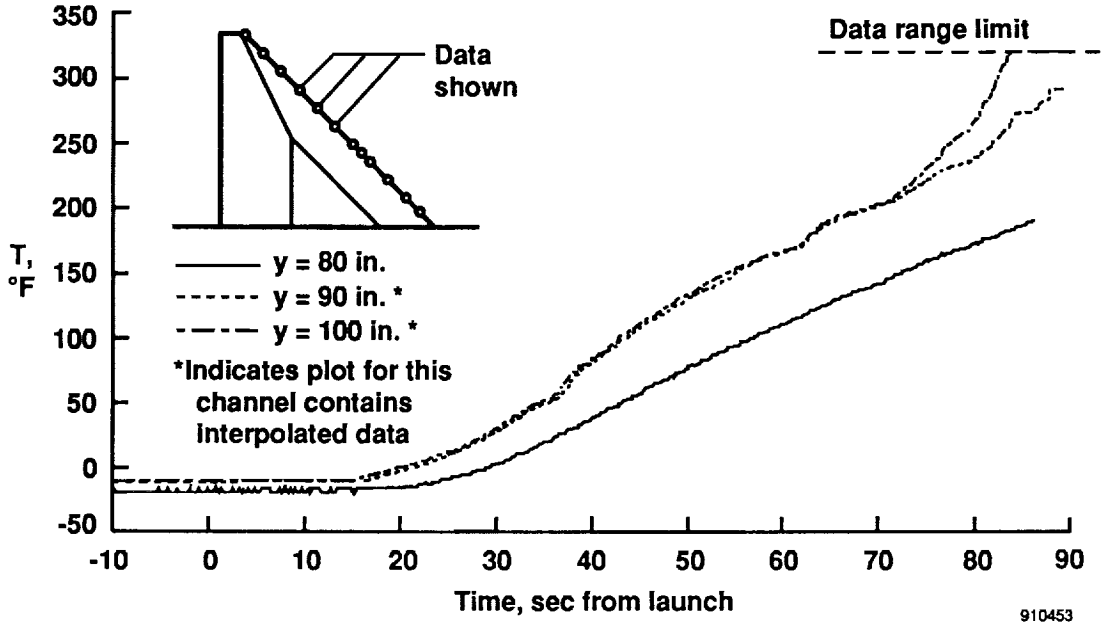

(c) y = 80, 90, and 100 in.

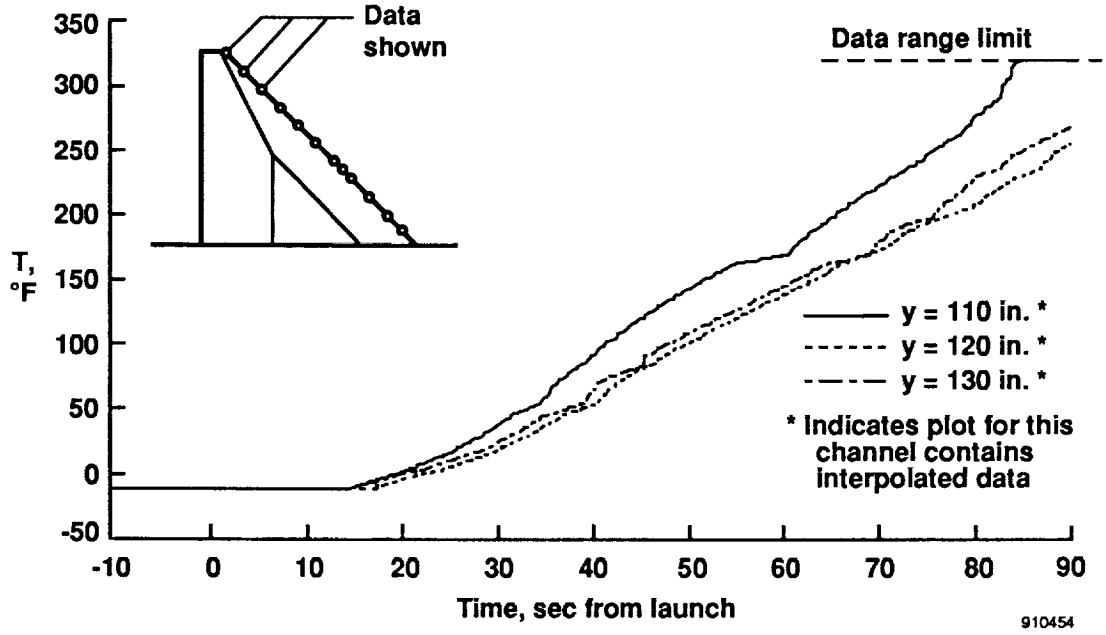

(d) y = 110, 120, and 130 in.

Figure 14. Concluded.

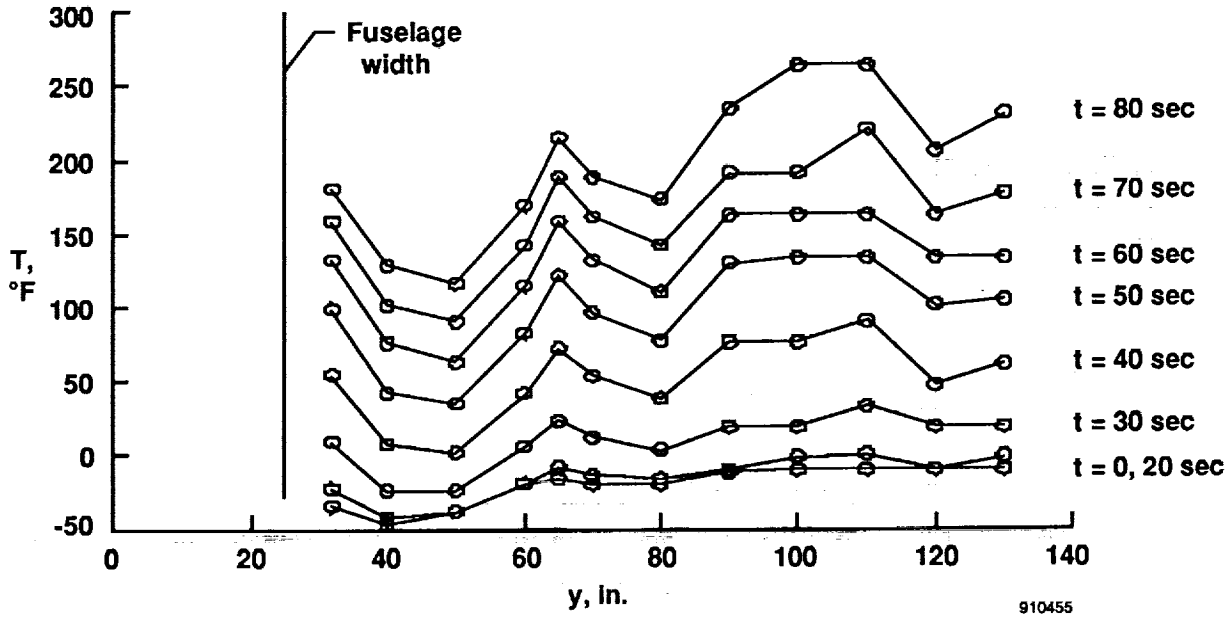

Figure 15. Spanwise distribution of wing leading-edge temperatures at half depth of Firex, °F.

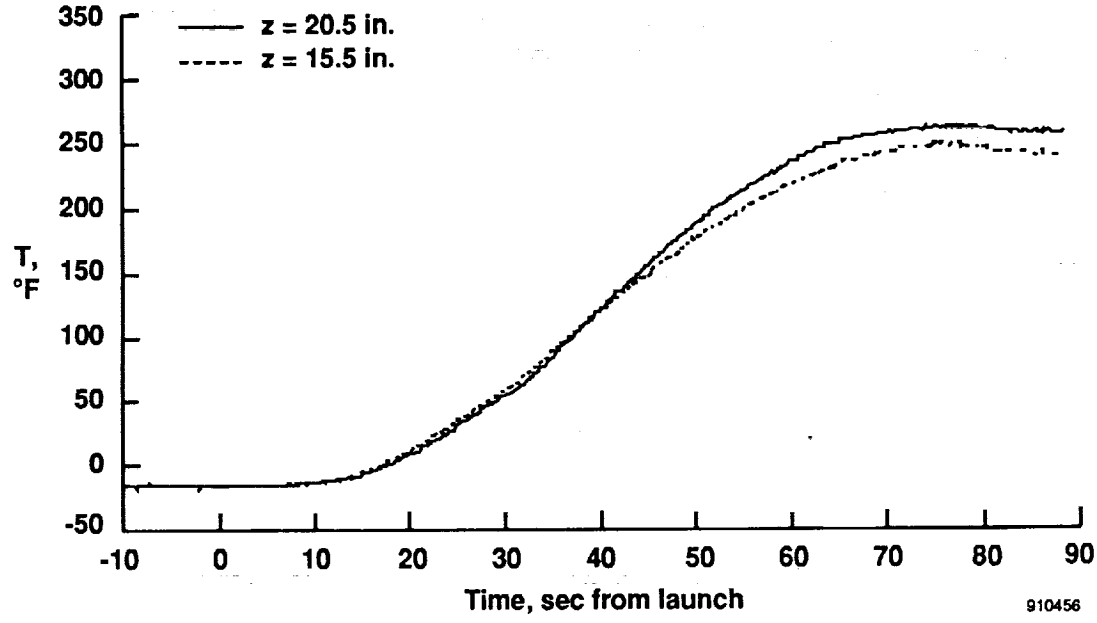

(a) FS = 288.4 in.

Figure 16. Fillet sidewall temperatures at the Thermolag–cork interface, °F.

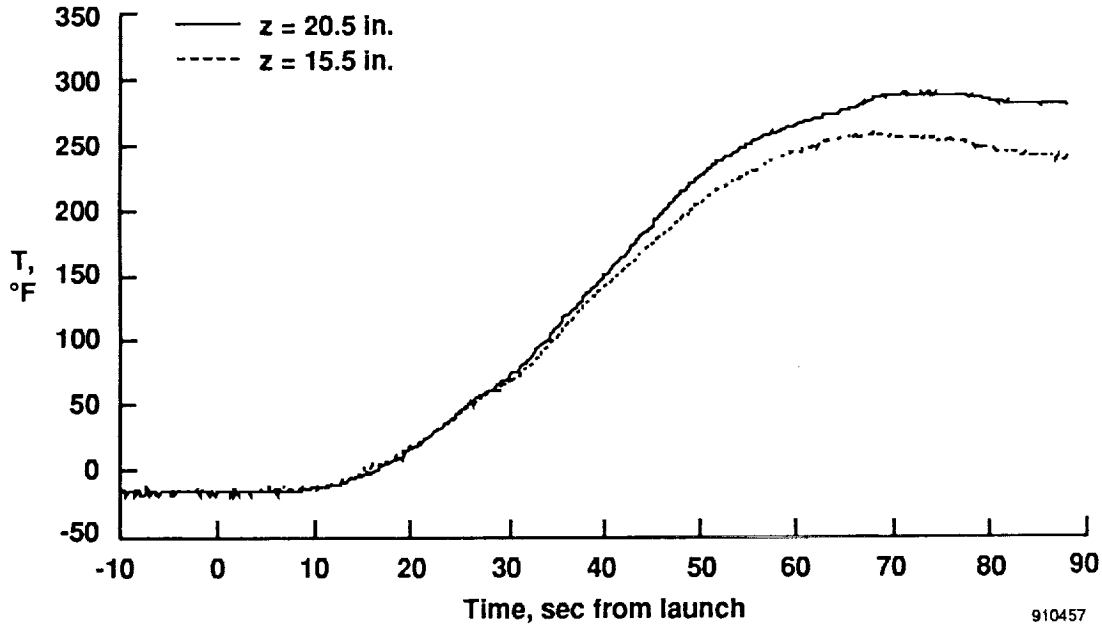

(b) FS = 280.6 in.

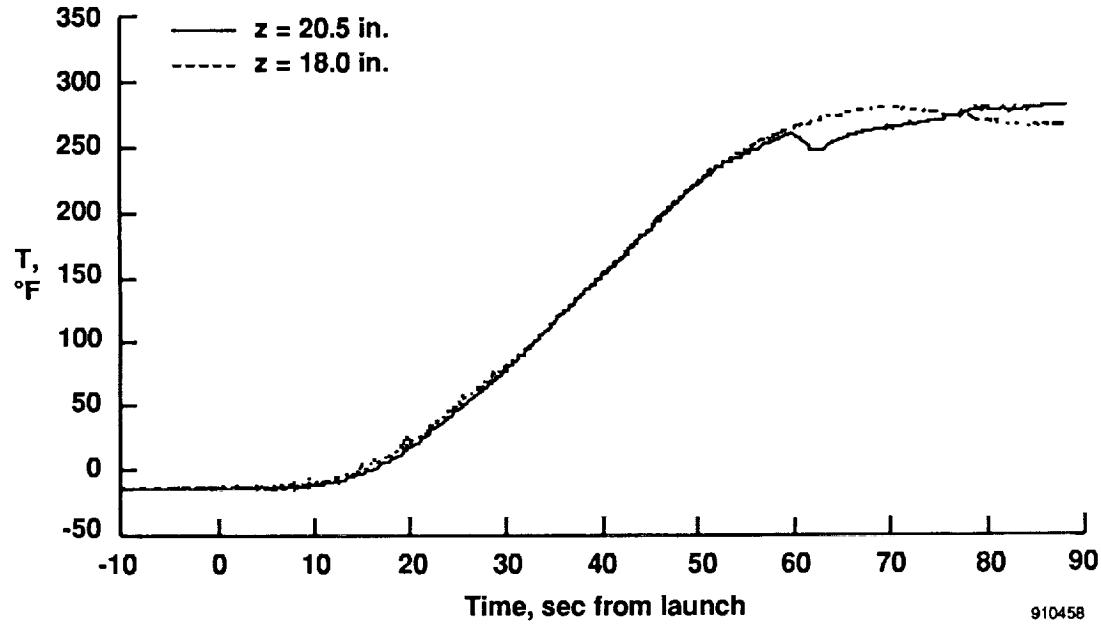

(c) FS = 270.4 in.

Figure 16. Continued.

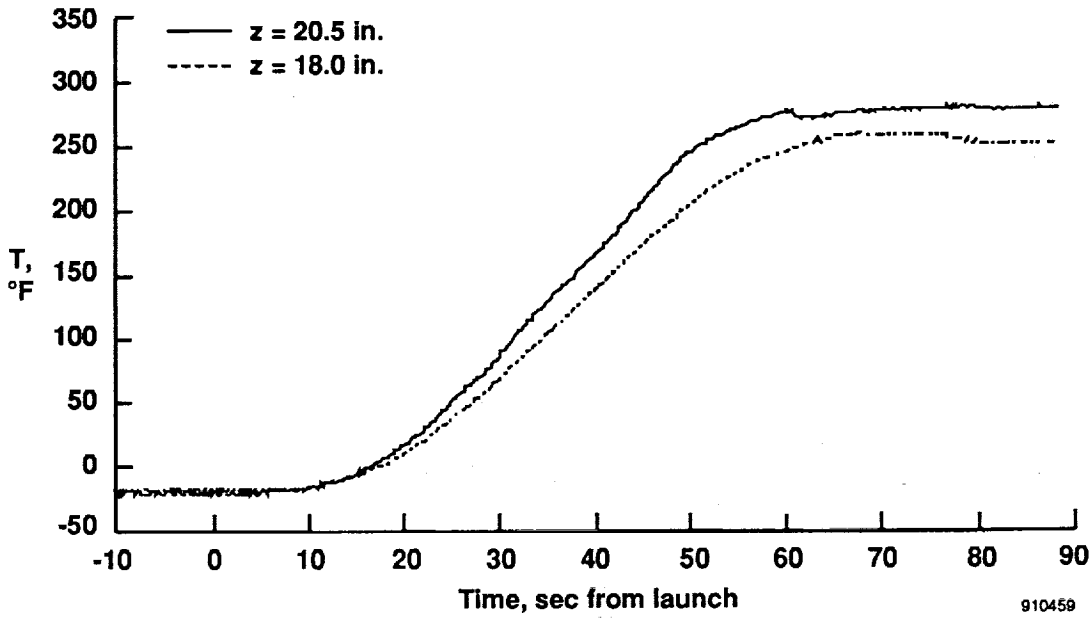

(d) FS = 263.5 in.

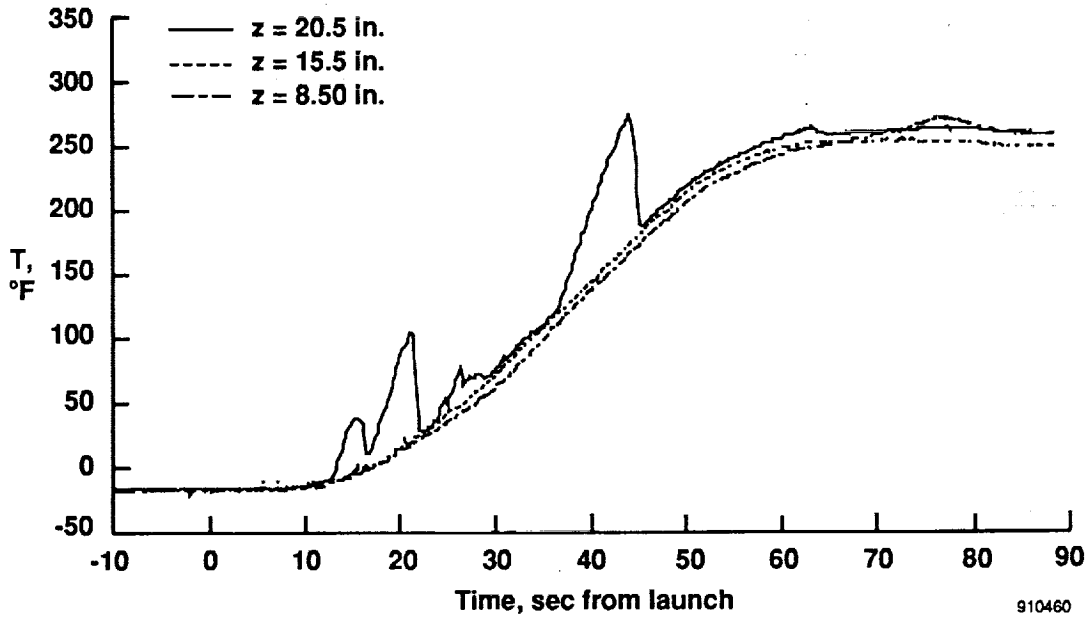

(e) FS = 253.1 in.

Figure 16. Continued.

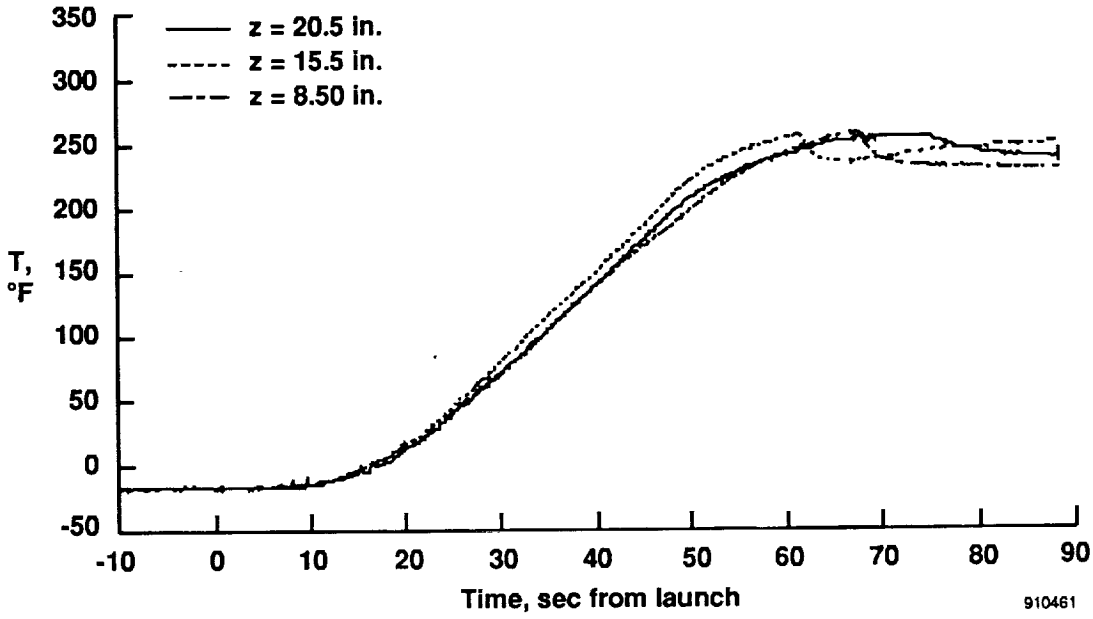

(f) FS = 246.2 in.

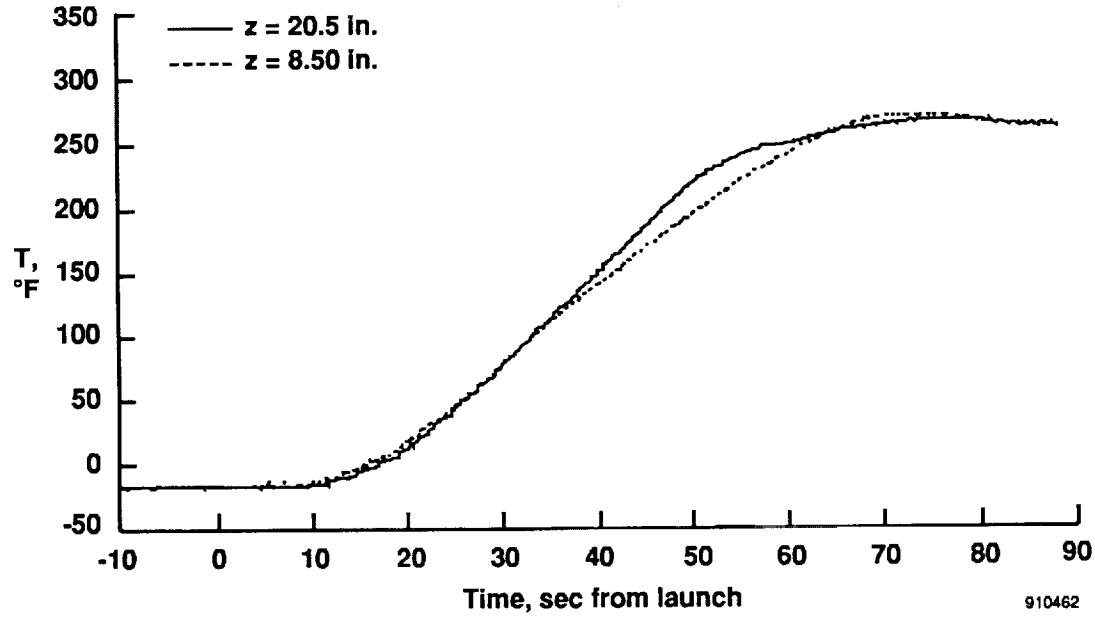

(g) FS = 241.0 in.

Figure 16. Concluded.

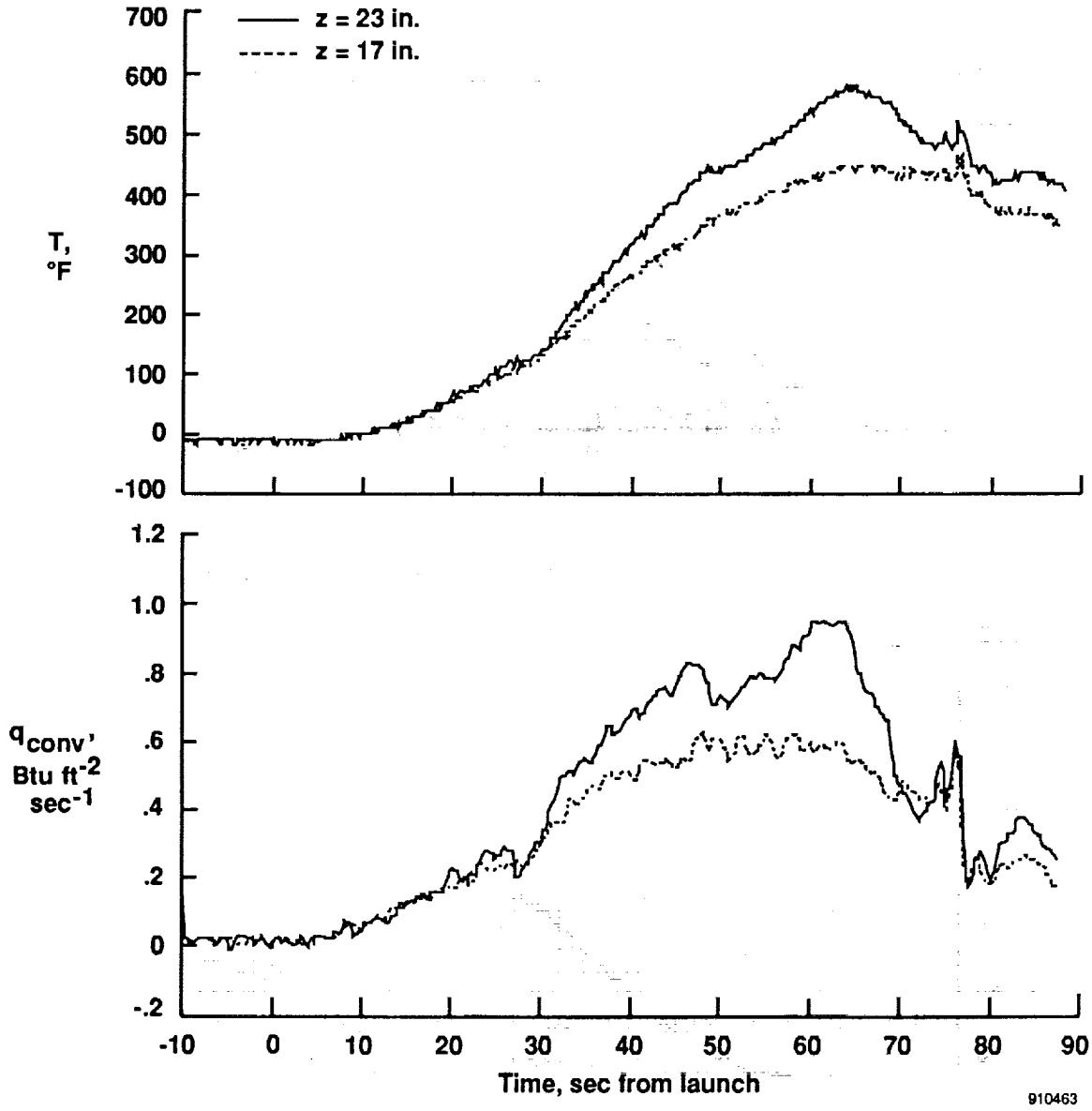

(a) FS = 288.4 in.

Figure 17. HRSI plug surface temperature data and derived heat flux estimates.

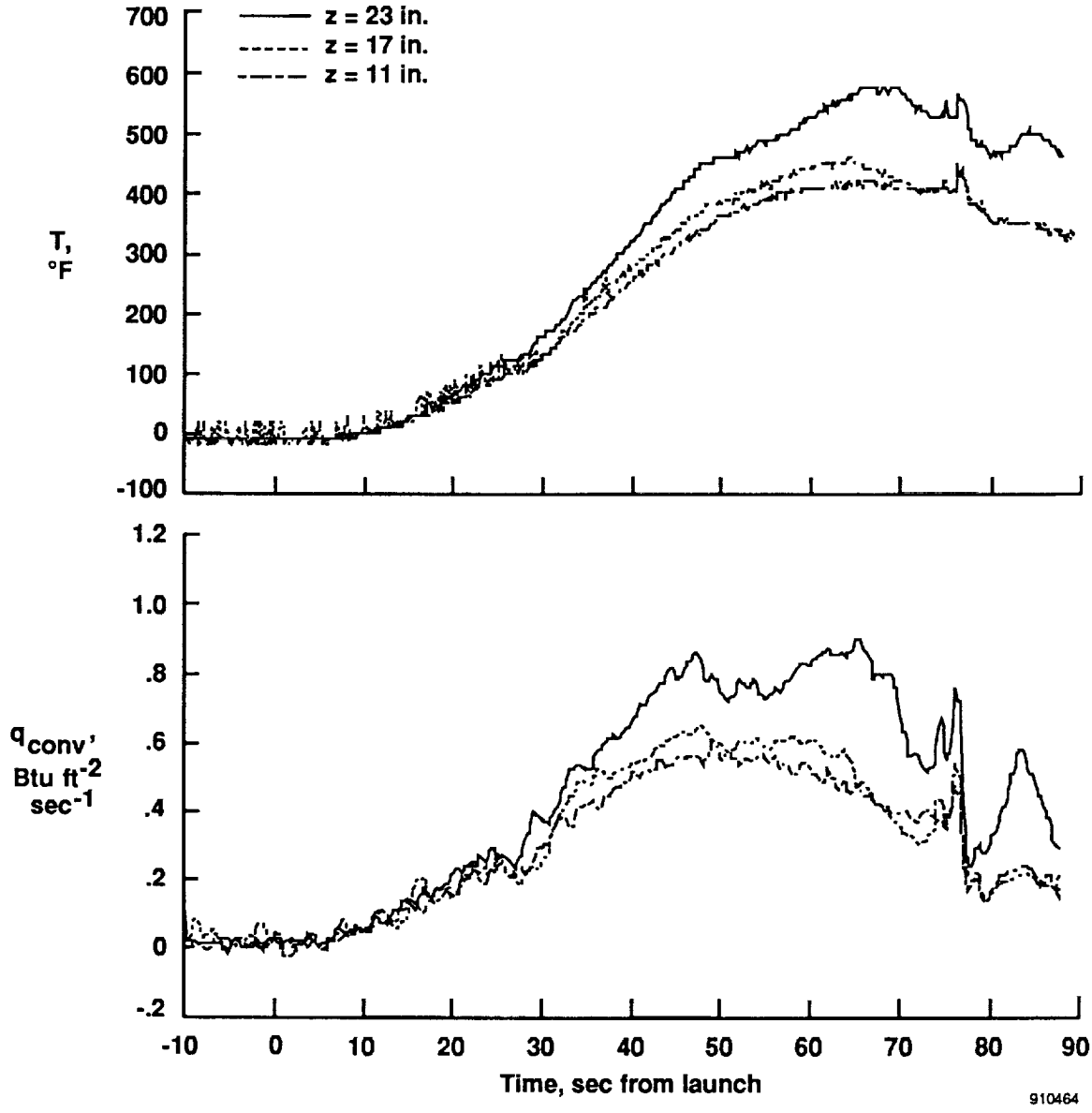

(b) FS = 280.6 in.

Figure 17. Continued.

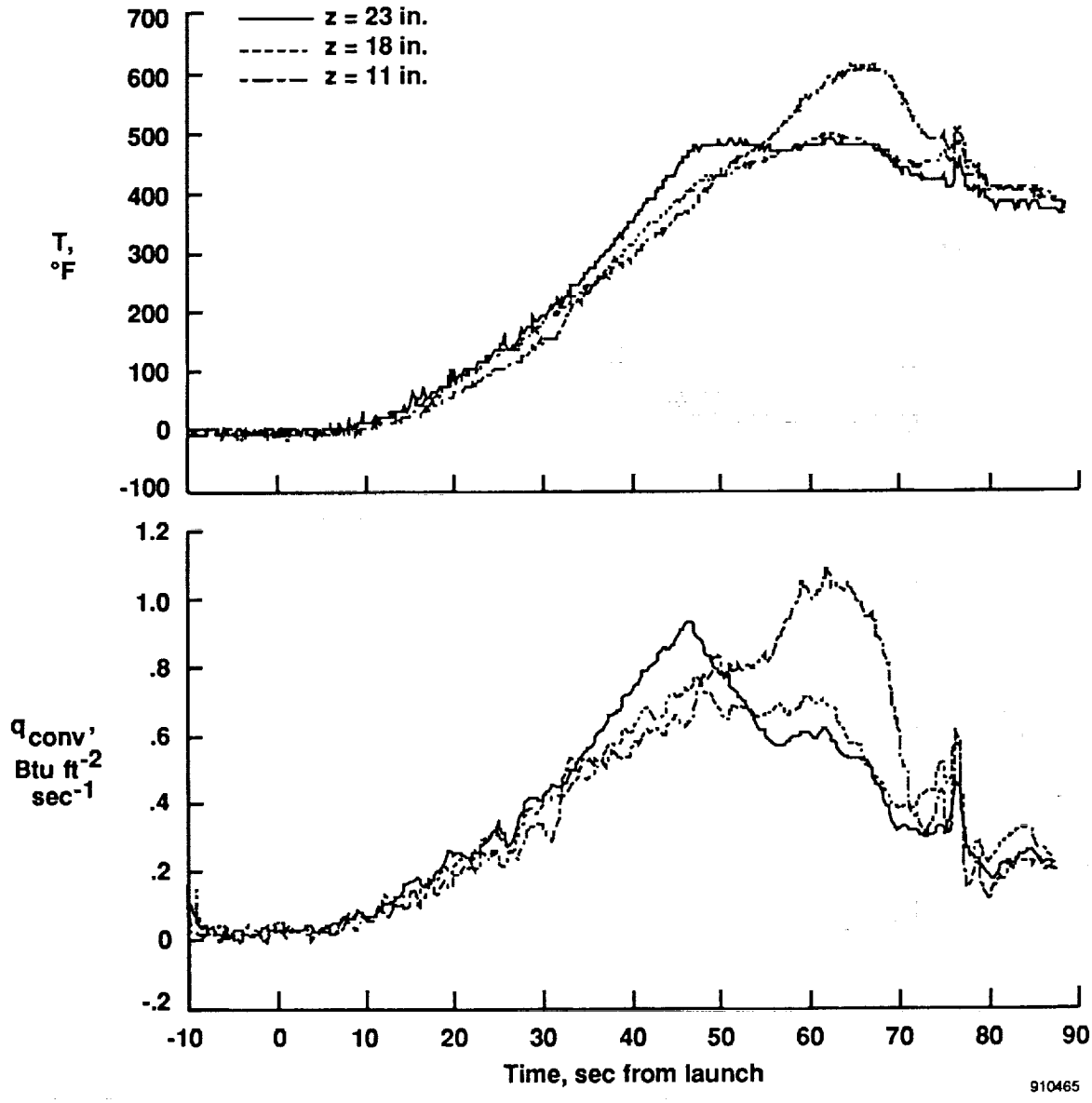

(c) FS = 253.1 in.

Figure 17. Continued.

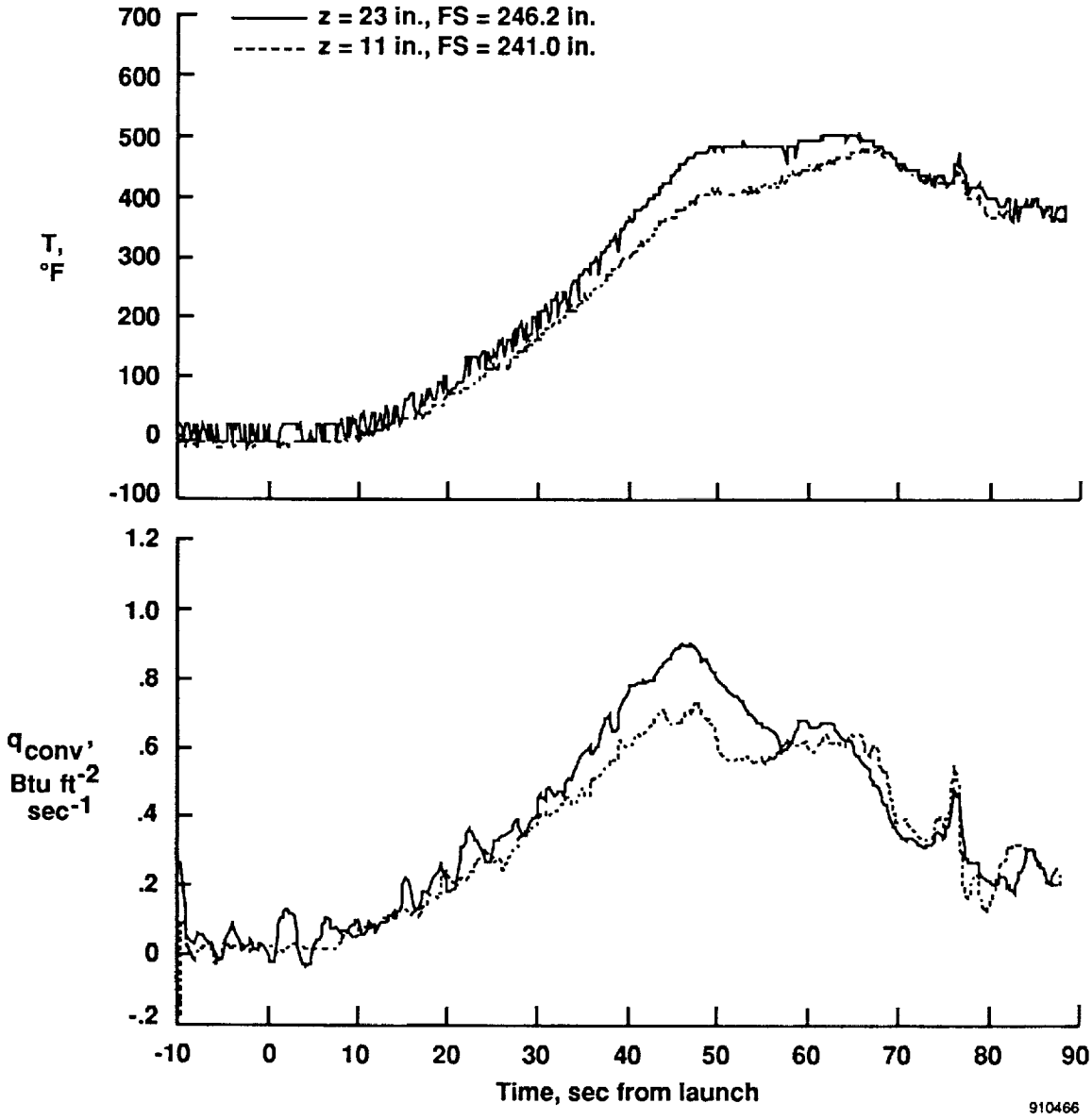

(d) FS = 246.2 and 241.0 in.

Figure 17. Concluded.

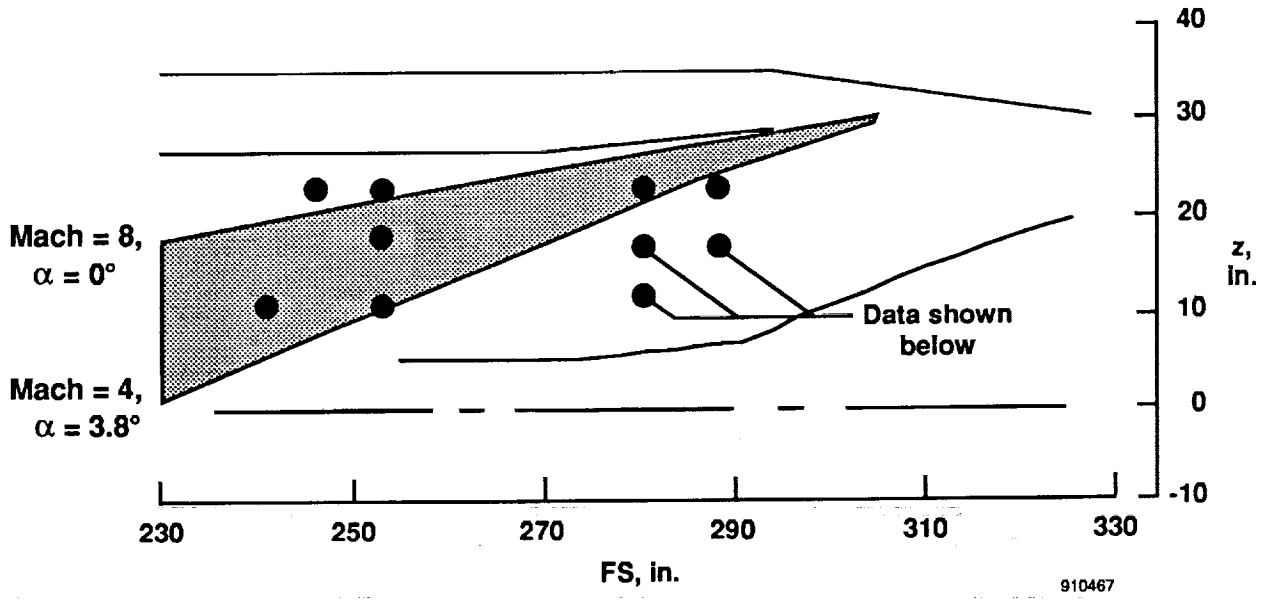

(a) Estimated wing leading-edge shock location, projected on fillet sidewall, two-dimensional wedge theory.

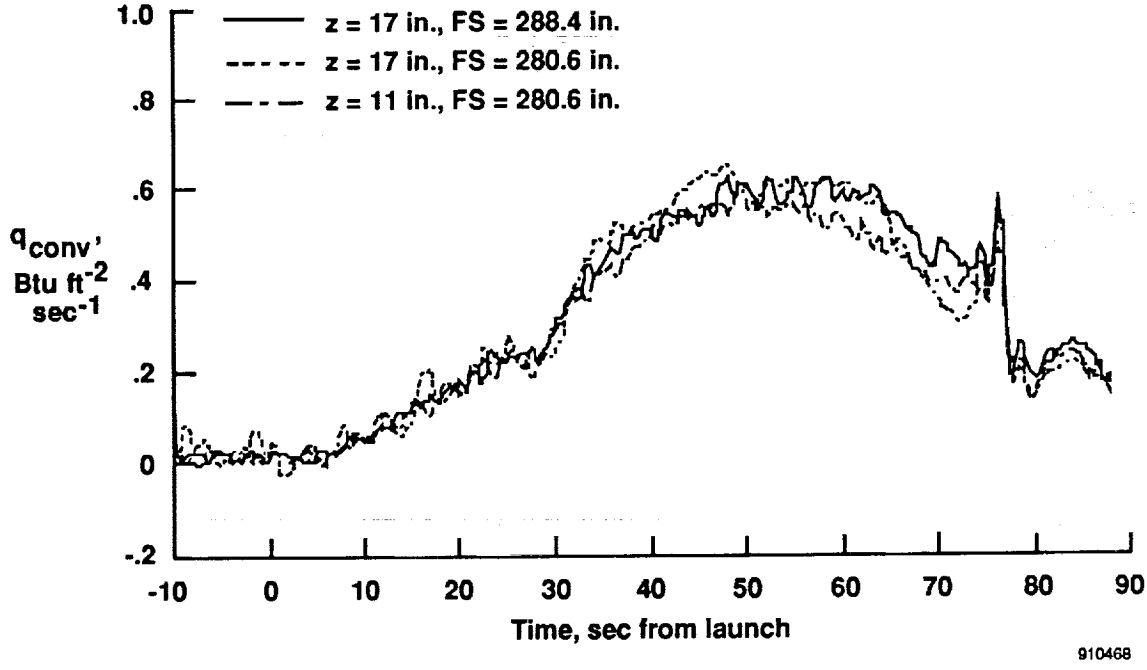

(b) Comparison of heat flux data, forward of estimated shock position.

Figure 18. Fillet sidewall reference heating.

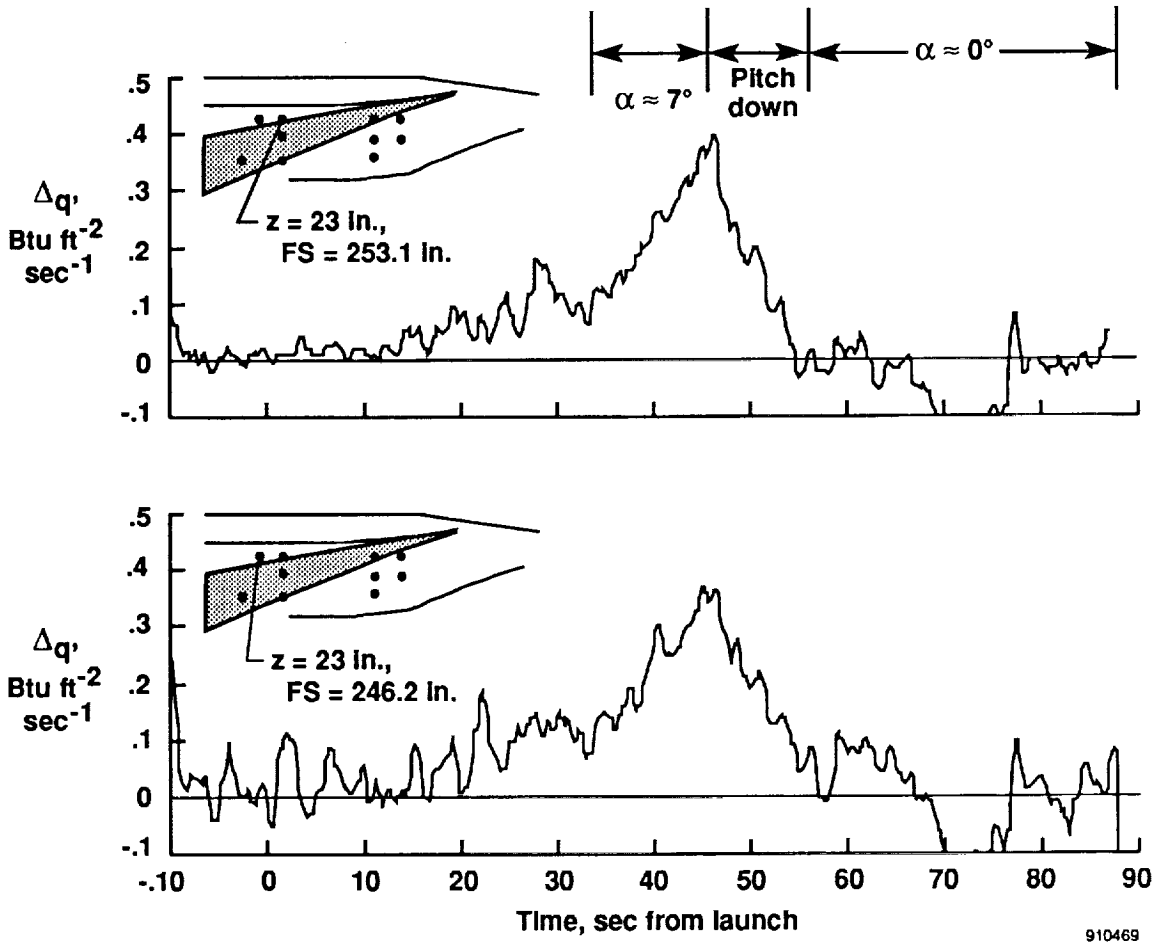

Figure 19. Fillet sidewall heating, aft of shock.

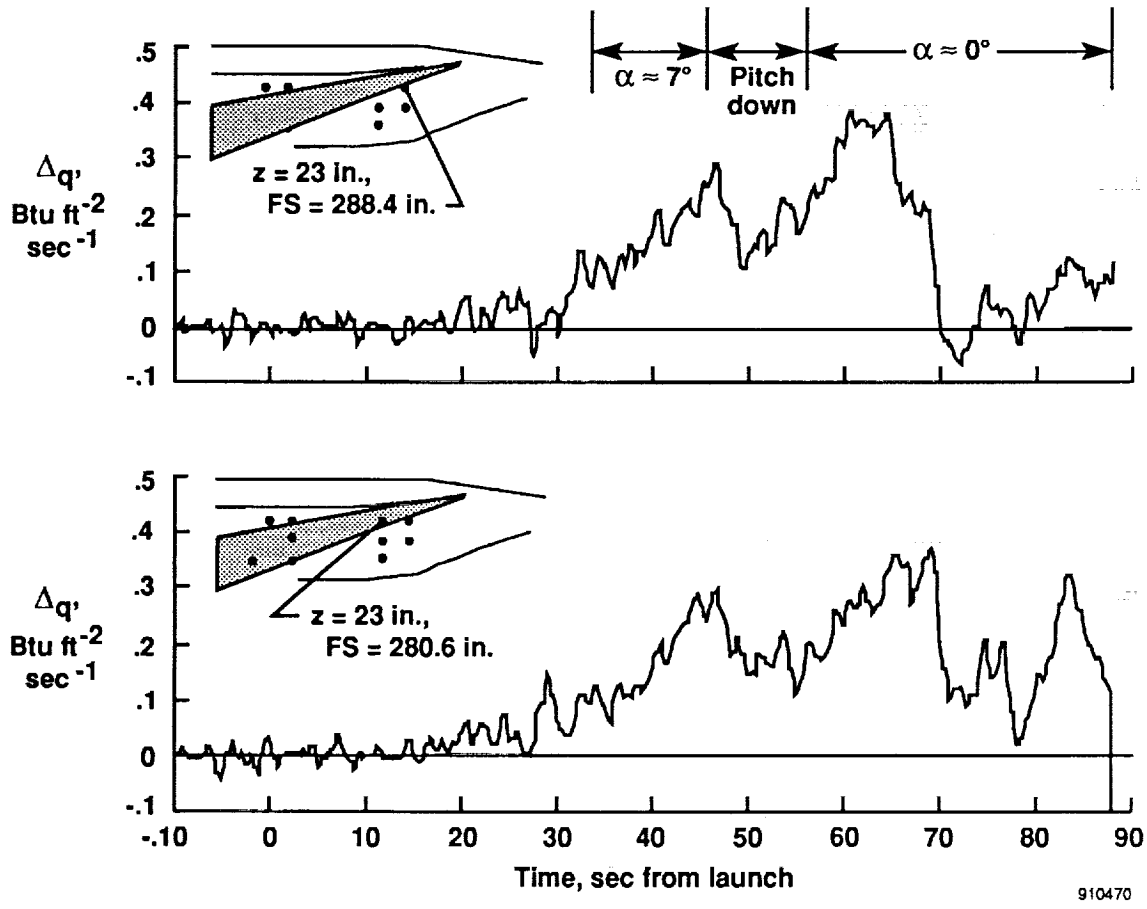

(a) FS = 288.4 in., z = 23 in.; FS = 280.6 in., z = 23 in.

Figure 20. Fillet sidewall heating in the vicinity of the wing leading-edge shock.

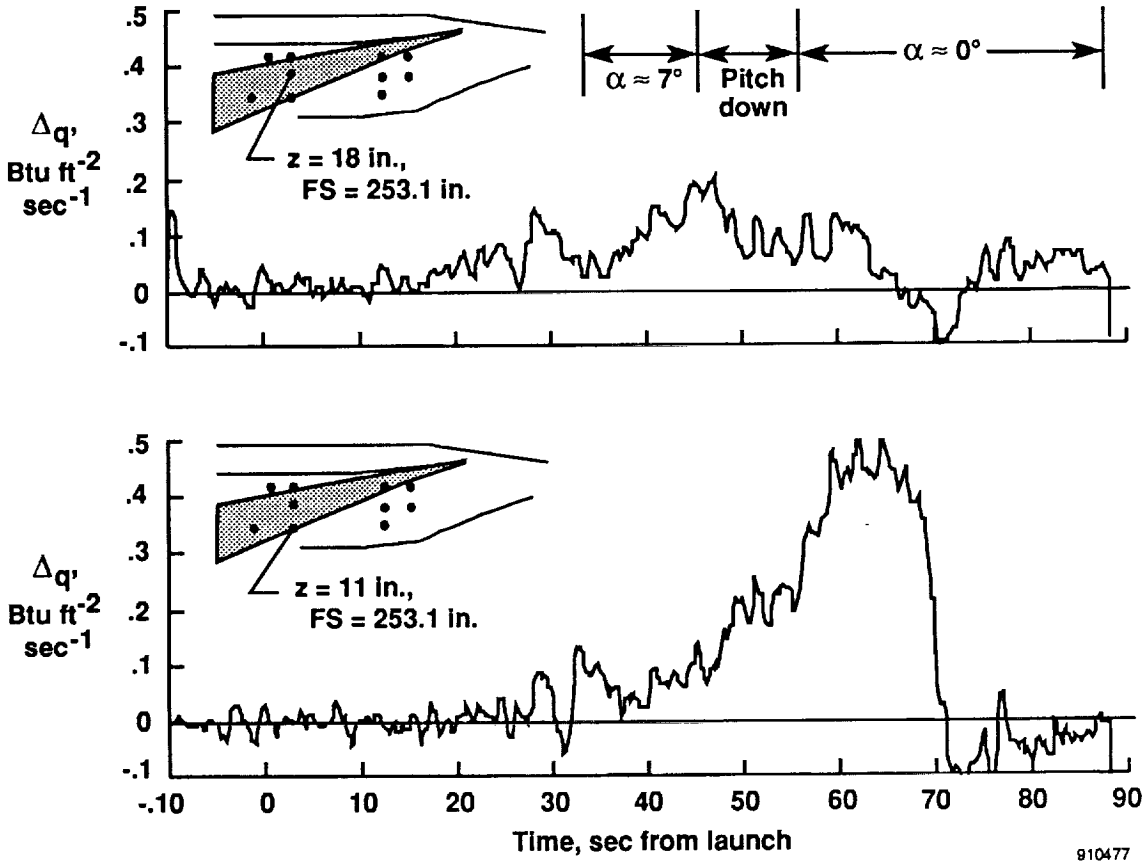

(b) FS = 253.1 in., z = 18 in.; FS = 253.1 in., z = 11 in.

Figure 20. Continued.

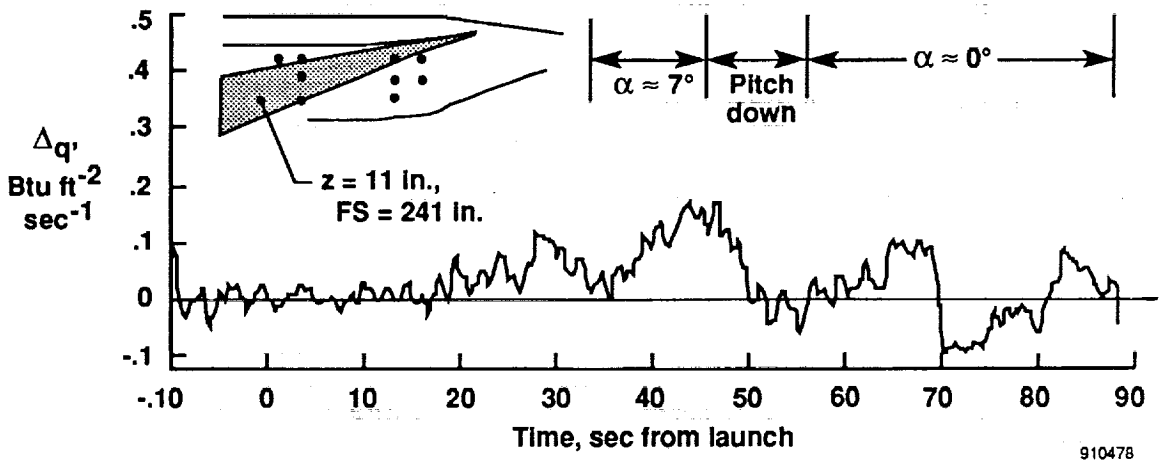

(c) FS = 241.0 in., z = 11 in.

Figure 20. Concluded.

REPORT DOCUMENTATION PAGE

Form Approved
OMB No. 0704-0188

1. AGENCY USE ONLY *(Leave blank)*	2. REPORT DATE	3. REPORT TYPE AND DATES COVERED
	October 1991	Technical Memorandum

4. TITLE AND SUBTITLE

Aerothermal Test Results From the First Flight of the Pegasus Air-Launched Space Booster

5. FUNDING NUMBERS

WU-505-59-40

6. AUTHOR(S)

Gregory K. Noffz, Robert E. Curry, Edward A. Haering, Jr. (Dryden Flight Research Facility, Edwards, California)
Paul Kolodziej (Ames Research Center, Moffett Field, California)

7. PERFORMING ORGANIZATION NAME(S) AND ADDRESS(ES)

NASA Dryden Flight Research Facility
P.O. Box 273
Edwards, California 93523-0273

8. PERFORMING ORGANIZATION REPORT NUMBER

H-1672

9. SPONSORING/MONITORING AGENCY NAME(S) AND ADDRESS(ES)

National Aeronautics and Space Administration
Washington, DC 20546-0001

10. SPONSORING/MONITORING AGENCY REPORT NUMBER

NASA TM-4330

11. SUPPLEMENTARY NOTES

12a. DISTRIBUTION/AVAILABILITY STATEMENT

Unclassified — Unlimited
Subject Category 34

12b. DISTRIBUTION CODE

13. ABSTRACT *(Maximum 200 words)*

A survey of temperature measurements was obtained at speeds through Mach 8.0 on the first flight of the Pegasus® air-launched booster system. In addition, heating rates were derived from the temperature data obtained on the fuselage in the vicinity of the wing shock interaction. Sensors were distributed on the wing surfaces, leading edge, and on the wing-body fairing or fillet. The majority of sensors were thin foil temperature gages installed near the surface within the vehicle's thermal protection system. In regions below the thermal protection system, standard bulb thermocouples were employed. In addition to these gages, thermocouples were installed on the surface of nonablating plugs. These sensors were more responsive to changes in flight conditions than the foil gages and allowed a derivation of convective heat flux. Side-by-side evaluations were obtained for a variety of sensor installations. Details of the trajectory reconstruction through first-stage separation are provided. This paper provides indepth descriptions of the sensor installations, temperature measurements, and derived heating rates along with interpretations of the results.

®Pegasus is a registered trademark of Orbital Sciences Corp., Fairfax, Virginia.

14. SUBJECT TERMS

Ablation; Flight-measured heat flux; Flight test techniques; Thermal protection system flight test

15. NUMBER OF PAGES

52

16. PRICE CODE

A04

17. SECURITY CLASSIFICATION OF REPORT	18. SECURITY CLASSIFICATION OF THIS PAGE	19. SECURITY CLASSIFICATION OF ABSTRACT	20. LIMITATION OF ABSTRACT
Unclassified	Unclassified		

NSN 7540-01-280-5500

Standard Form 298 (Rev. 2-89)
Prescribed by ANSI Std. Z39-18
298-102